JGR Atmospheres

RESEARCH ARTICLE
10.1029/2019JD031224

Mie Scattering Captures Observed Optical Properties of Ambient Biomass Burning Plumes Assuming Uniform Black, Brown, and Organic Carbon Mixtures

Petr Chylek[1], James E. Lee[1], Dian E. Romonosky[1,2], Francesca Gallo[1], Sijia Lou[3], Manish Shrivastava[3], Christian M. Carrico[1,4], Allison C. Aiken[1], and Manvendra K. Dubey[1]

[1]Earth and Environmental Sciences, Los Alamos National Laboratory, Los Alamos, NM, USA, [2]Department of Chemistry, State University of New York at Geneseo, Geneseo, NY, USA, [3]Pacific Northwest National Laboratory, Richland, WA, USA, [4]Department of Civil and Environmental Engineering, New Mexico Institute of Mining and Technology, Socorro, NM, USA

Key Points:
- Mie scattering model assuming spherical aerosol particles captures basic optical properties of ambient biomass burning aerosols
- Absorption Ångström exponent (AAE) of black carbon is limited to AAE <1.4, and AAE values >1.7 require the presence of brown carbon
- The imaginary part of refractive index of brown carbon at the blue end of a solar spectrum is found to be between 0.005 and 0.016 for ambient plumes

Correspondence to:
P. Chylek,
chylek@lanl.gov

Citation:
Chylek, P., Lee, J. E., Romonosky, D. E., Gallo, F., Lou, S., Shrivastava, M., et al. (2019). Mie scattering captures observed optical properties of ambient biomass burning plumes assuming uniform black, brown, and organic carbon mixtures. *Journal of Geophysical Research: Atmospheres*, *124*, 11,406–11,427. https://doi.org/10.1029/2019JD031224

Received 23 JUN 2019
Accepted 10 SEP 2019
Accepted article online 13 SEP 2019
Published online 6 NOV 2019

Author Contributions:
Conceptualization: Petr Chylek, Allison C. Aiken, Manvendra K. Dubey
Data curation: Dian E. Romonosky, Francesca Gallo, Allison C. Aiken
Formal analysis: Petr Chylek, James E. Lee, Francesca Gallo
Investigation: Petr Chylek, James E. Lee
Methodology: Dian E. Romonosky, Sijia Lou, Manish Shrivastava, Manvendra K. Dubey
Project administration: Manvendra K. Dubey
Resources: Dian E. Romonosky
(continued)

Abstract We use a simple model of a spherical biomass burning aerosol particle containing an internal mixture of black carbon (BC) and organic carbon (OC) with an effective refractive index calculated as a volume fraction-weighted mean of refractive indices. Brown carbon (BrC) is considered to be an OC with an imaginary part of refractive index at the blue end of the solar spectrum higher (in absolute value) than at the red end. Mie-scattering formalism is employed to calculate absorption Ångström exponent (AAE) as a function of single-scattering albedo (SSA) for a set of BC refractive indices, BC volume fraction, and a set of effective refractive indices of BC and BrC mixtures. Ambient plumes are characterized by their mean SSA at 405 nm wavelength and two-wavelength (405 and 781 nm) AAE values. Comparing observed and model-calculated AAE and SSA values identifies the BC refractive index and its volume fraction and an effective refractive index of the BC and BrC mixture. From these values, the imaginary part of BrC refractive index is calculated. For observed southwestern ambient fires, the imaginary part of BrC refractive index is ≤0.016. In contrast, fires in the Amazon and from Africa are dominated by BC. We also use the Mie scattering model to establish the upper limit on AAE of BC (AAE ≤ 1.4) and the upper limit of the BC and OC mixture (AAE ≤ 1.7). Any AAE(405/781) > 1.7 requires the presence of BrC. We derive several relationships between AAE, SSA, BC fractions, and an imaginary part of BrC refractive index of ambient fires.

1. Introduction

Biomass burning produces light-absorbing aerosol containing a mixture of black carbon (BC) and organic carbon (OC). When OC absorbs more strongly at the blue end of solar spectrum than at the red end, it is called brown carbon (BrC) due to its brownish appearance. The exact configuration of BC and OC within the aerosol is highly variable over geography and time. To represent realistically the radiative properties of such composite aerosols in climate models is not an easy task. Furthermore, the amount and the chemical composition of BrC emitted is unknown and it is often inferred from measured optical properties of mixed carbonaceous aerosols.

A mixture of materials can exist as an external mixture, where there are separate particles of BC and OC, or as an internal mixture, where the BC and OC are within one aerosol particle. The internal mixture can be either quasi-homogeneous or it can have a specified heterogeneous structure. The optical properties of homogeneous internal mixtures are usually characterized by an effective refractive index. There are several prescriptions, called mixing rules (e.g., Chylek et al., 1988; Chylek & Srivastava, 1983; Liu et al., 2014; Videen & Chylek, 1998), that provide means to calculate the effective refractive index of the mixture given the refractive indices and volume fractions of the individual components. The simplest mixing rules use volume-fraction-weighted averages of the individual refractive indices or dielectric constants. A little more complicated are the Bruggeman (1936) and Maxwell (1904) mixing rules based on the mean field theory with different geometrical distribution of individual components. The effective refractive index is expected to transform a complex untraceable situation with many different particle shapes, compositions, and morphologies into an easily manageable case where complex structures are represented by a single complex parameter called

JGR Atmospheres

RESEARCH ARTICLE
10.1029/2019JD031224

Mie Scattering Captures Observed Optical Properties of Ambient Biomass Burning Plumes Assuming Uniform Black, Brown, and Organic Carbon Mixtures

Petr Chylek[1], James E. Lee[1], Dian E. Romonosky[1,2], Francesca Gallo[1], Sijia Lou[3], Manish Shrivastava[3], Christian M. Carrico[1,4], Allison C. Aiken[1], and Manvendra K. Dubey[1]

[1]Earth and Environmental Sciences, Los Alamos National Laboratory, Los Alamos, NM, USA, [2]Department of Chemistry, State University of New York at Geneseo, Geneseo, NY, USA, [3]Pacific Northwest National Laboratory, Richland, WA, USA, [4]Department of Civil and Environmental Engineering, New Mexico Institute of Mining and Technology, Socorro, NM, USA

Abstract We use a simple model of a spherical biomass burning aerosol particle containing an internal mixture of black carbon (BC) and organic carbon (OC) with an effective refractive index calculated as a volume fraction-weighted mean of refractive indices. Brown carbon (BrC) is considered to be an OC with an imaginary part of refractive index at the blue end of the solar spectrum higher (in absolute value) than at the red end. Mie-scattering formalism is employed to calculate absorption Ångström exponent (AAE) as a function of single-scattering albedo (SSA) for a set of BC refractive indices, BC volume fraction, and a set of effective refractive indices of BC and BrC mixtures. Ambient plumes are characterized by their mean SSA at 405 nm wavelength and two-wavelength (405 and 781 nm) AAE values. Comparing observed and model-calculated AAE and SSA values identifies the BC refractive index and its volume fraction and an effective refractive index of the BC and BrC mixture. From these values, the imaginary part of BrC refractive index is calculated. For observed southwestern ambient fires, the imaginary part of BrC refractive index is ≤0.016. In contrast, fires in the Amazon and from Africa are dominated by BC. We also use the Mie scattering model to establish the upper limit on AAE of BC (AAE ≤ 1.4) and the upper limit of the BC and OC mixture (AAE ≤ 1.7). Any AAE(405/781) > 1.7 requires the presence of BrC. We derive several relationships between AAE, SSA, BC fractions, and an imaginary part of BrC refractive index of ambient fires.

Key Points:
- Mie scattering model assuming spherical aerosol particles captures basic optical properties of ambient biomass burning aerosols
- Absorption Ångström exponent (AAE) of black carbon is limited to AAE <1.4, and AAE values >1.7 require the presence of brown carbon
- The imaginary part of refractive index of brown carbon at the blue end of a solar spectrum is found to be between 0.005 and 0.016 for ambient plumes

Correspondence to:
P. Chylek,
chylek@lanl.gov

Citation:
Chylek, P., Lee, J. E., Romonosky, D. E., Gallo, F., Lou, S., Shrivastava, M., et al. (2019). Mie scattering captures observed optical properties of ambient biomass burning plumes assuming uniform black, brown, and organic carbon mixtures. *Journal of Geophysical Research: Atmospheres*, *124*, 11,406–11,427. https://doi.org/10.1029/2019JD031224

Received 23 JUN 2019
Accepted 10 SEP 2019
Accepted article online 13 SEP 2019
Published online 6 NOV 2019

Author Contributions:
Conceptualization: Petr Chylek, Allison C. Aiken, Manvendra K. Dubey
Data curation: Dian E. Romonosky, Francesca Gallo, Allison C. Aiken
Formal analysis: Petr Chylek, James E. Lee, Francesca Gallo
Investigation: Petr Chylek, James E. Lee
Methodology: Dian E. Romonosky, Sijia Lou, Manish Shrivastava, Manvendra K. Dubey
Project administration: Manvendra K. Dubey
Resources: Dian E. Romonosky
(continued)

1. Introduction

Biomass burning produces light-absorbing aerosol containing a mixture of black carbon (BC) and organic carbon (OC). When OC absorbs more strongly at the blue end of solar spectrum than at the red end, it is called brown carbon (BrC) due to its brownish appearance. The exact configuration of BC and OC within the aerosol is highly variable over geography and time. To represent realistically the radiative properties of such composite aerosols in climate models is not an easy task. Furthermore, the amount and the chemical composition of BrC emitted is unknown and it is often inferred from measured optical properties of mixed carbonaceous aerosols.

A mixture of materials can exist as an external mixture, where there are separate particles of BC and OC, or as an internal mixture, where the BC and OC are within one aerosol particle. The internal mixture can be either quasi-homogeneous or it can have a specified heterogeneous structure. The optical properties of homogeneous internal mixtures are usually characterized by an effective refractive index. There are several prescriptions, called mixing rules (e.g., Chylek et al., 1988; Chylek & Srivastava, 1983; Liu et al., 2014; Videen & Chylek, 1998), that provide means to calculate the effective refractive index of the mixture given the refractive indices and volume fractions of the individual components. The simplest mixing rules use volume-fraction-weighted averages of the individual refractive indices or dielectric constants. A little more complicated are the Bruggeman (1936) and Maxwell (1904) mixing rules based on the mean field theory with different geometrical distribution of individual components. The effective refractive index is expected to transform a complex untraceable situation with many different particle shapes, compositions, and morphologies into an easily manageable case where complex structures are represented by a single complex parameter called

Software: Sijia Lou, Manish Shrivastava
Supervision: Petr Chylek
Writing - original draft: Petr Chylek
Writing – review & editing: Manvendra K. Dubey

the effective refractive index. This is an ad hoc mean state treatment rather than approximation in a mathematical sense where the accuracy can be estimate by considering contributions of neglected terms (Chylek et al., 2000).

A heterogeneous internal mixture is usually represented by a core containing BC surrounded by a shell of less absorbing material (e.g., Kanngiesser & Kahnert, 2018). Although this core-shell model seems to be in agreement with our mental picture of the aged biomass burning aerosols, its disadvantage is an increasing number of free parameters, and results which do not seem to rank this model much better than a simple homogeneous sphere model (Cappa et al., 2019; China et al., 2015; Curci et al., 2019; Kahnert et al., 2012; Lesins et al., 2002; Schuster et al., 2016). Although theoretical method to obtain scattering characteristics of nonspherical particles and particle groups are available (e.g., He et al., 2016; Mishchenko, 2014; Mishchenko et al., 1995; Videen et al., 1995 Yang et al., 2019), we concentrate in the following analysis on the simple Mie scattering model.

Lesins et al. (2002) compared optical properties calculated using internal mixtures where the effective refractive index was obtained using different mixing rules. The conclusion was that for the case of BC and OC, the different mixing rules have a minor effect on the derived optical properties. The results varied within 5% from each other, and the volume averaging of refractive indices was found to be a reasonable approximation. The differences between optical properties of a homogeneous sphere with an effective refractive index and the layered sphere model were within 20%. Similar results were obtained by Kahnert et al. (2012). They found that the volume averaging of refractive indices works reasonably well, only slightly worse than the Maxwell-Garnett mixing rule. In addition, Kahnert et al. found that the homogeneous sphere model provided more accurate results than the layered sphere model. Similarly, Torok et al. (2018) suggested that soot core and coating is not a good model for laboratory-produced soot.

China et al. (2015) investigated soot particles transported over long distances. Particle sizes and shapes were determined using electron microscopy. They found over 70% of particles to be highly compacted with only about 25% having a core-shell geometry. The radiative forcing estimate using a simple Mie scattering calculation was within 12% (China et al., 2015) of that using the discrete dipole approximation (Draine & Flatau, 1994). Fierce et al. (2017) found that a fully mixed approximation provides an accurate estimate of the scattering coefficient, but overestimates absorption. Several investigators analyzing Brazilian biomass burning aerosols (Martins et al., 1998; Schmid et al., 2009) concluded that aerosols from the Amazon Basin are reasonably spherical with the dominating diameter between 200 and 500 nm (Rissler et al., 2006; Schmid et al., 2006; Schmid et al., 2009). Curci et al. (2019) tested several combinations of external and internal mixing. One test consisted of homogeneous mixing of all species including BC. Another test included a core-shell configuration. Although they considered the first model unrealistic and the second physically plausible, the results of those two tests were very similar. Thus, there is no clear evidence that more complicated models provide better approximations to the optical properties of biomass burning smoke than simple homogeneous particles with an effective refractive index and spherical geometry.

Bahadur et al. (2012) demonstrated that BrC is an important component for absorption of solar radiation. As such, BrC can potentially alter the direct radiative forcing by aerosols. The strength of the absorption of BrC is determined by the imaginary part of its refractive index. Chakrabarty et al. (2010) found in laboratory experiments the imaginary part of BrC smoke refractive index to be 0.015 for ponderosa pine and 0.0076 for Alaskan duff. Similarly, Sumlin et al. (2018) reports imaginary part of BrC refractive index at 375 nm to be 0.014. On the other hand, Kirchstetter et al. (2004) reported an imaginary part of BrC refractive index based on an analysis of biomass burning laboratory samples to be 0.112 at 400 nm, an order of magnitude higher than Chakrabarty's values. Similarly, high values of absorption near 400 nm were found by Barnard et al. (2008). Wang et al. (2014) summarized results of several research groups reporting the range of the imaginary part of the refractive index of BrC near 400 nm to be within the range of 0.01i to 0.20i. Sengupta et al. (2018) reports even a larger span of imaginary part of refractive indices of bulk biomass burning organic aerosols at 400 nm starting around 0.002i. Thus, the imaginary part of refractive index of BrC, which determines the strength of absorption of BrC near the blue end of solar spectrum, is uncertain by several orders of magnitude. This uncertainty due to absorption strength of BrC is much higher than a potential uncertainty due to mixing rules (~10%) or due to the specific morphology of carbonaceous aerosol particles (~50%). The goal of the following analysis is to deduce the imaginary part of the BrC refractive index at the blue end of solar spectrum, especially for smoke from southwestern U.S. forest fuels, using a simple Mie scattering model.

2. The Model

In the following, we use BC as a generic name for the soot with various degrees of carbonization reflected by specified values of the BC refractive index. The degree of carbonization depends on various factors including the material burned (chemical composition, water content, etc.), the temperature and the nature of the flame (smoldering or flaming), and on other environmental and laboratory factors. Although the absolute values of the imaginary part around 0.5 has been frequently used, some laboratory measurements (Habib & Vervisch, 1988) as well as analysis of biomass burning fires (Schmid et al., 2009) found values of an imaginary part of the refractive index of BC to be much lower (0.2 to 0.3), while others recommend much higher values up to 0.79 (Bond and Bergstrom, 2007). We consider values of the imaginary part of BC refractive index within the range between 0.1 and 0.5 as well as the value of 0.79. We find that 0.3 is the value compatible with most of the biomass burning plumes reported here. Thus, the assumption of BC refractive index of 1.5–0.3i for ambient fires can be considered a part of our model specification.

The OC is considered to have a refractive index that is a constant across the visible part of the solar spectrum. We take the real part of refractive index of OC to be $n = 1.46$ according to the analysis of Schmid et al. (2009). BrC is a special form of OC that absorbs sunlight with an imaginary part of the refractive index that is higher (in absolute value) at shorter blue wavelengths than at the red end of the solar spectrum. This higher absorption at blue wavelengths is responsible for the brownish appearance of some biomass burning plumes.

In creating a model of the biomass burning plumes, we keep simplicity in mind. A very complex model with many free (unknown) parameters may be less useful than a simple model with a minimum number of free parameters. A simple model may provide insights into relationship between different plume parameters that might not be apparent using a more complex model. We try to find a proper compromise between simplicity and accuracy.

Some of aerosol particles are nonspherical, especially from fresh combustion sources. However, averaging over all possible sizes, shapes, and orientations, together with biomass burning plume atmospheric aging, the spherical particle approximation is brought closer to reality. In addition, any model based on a given observed shape and composition captures just one specific configuration among many different possibilities and there is no guarantee that this one particular model will be closer to an average of all possibilities than a simple homogeneous spherical case. Considering complications by scattering and absorption by nonspherical and heterogeneous particles compared to the simplicity of the Mie scattering model, a simple model is justified among a collection of more complicated alternatives. Furthermore, these simple Mie codes are used in standard Intergovernmental Panel of Climate Change-class climate models and more complex core-shell models are usually used to evaluate sensitivities. We stress that core shell analysis is appropriate for the analysis of laboratory data such as Cross et al. (2010) where the configuration is well characterized and coating thickness and core size are systematically explored. It is also important to recognize that BC morphology and mixing is much more complex and variable with sources and regions. For example, field data in Sacramento, Fresno, and Fontana, California show a low absorption enhancement by coatings (Cappa et al., 2012, 2019) while some others are reporting large enhancement (Liu, Scheuer, et al., 2014). Concerning the state of modelling, Cappa et al. (2019) suggest that the amount of coating is likely overestimated by models and that the mixing-induced absorption enhancement (spherical core-shell model) might be overestimated to an even greater extent. A recent paper (McClure et al., 2019) reports a negligible coating enhancement in laboratory experiments.

We therefore decided to base our parsimonious model (a compromise between simplicity and accuracy) on an internal mixture of BC and OC with an effective refractive index of a mixture obtained by volume averaging of the refractive indices of its components. The scattering characteristics are obtained using the Mie scattering formulation assuming a spherical geometry. A similar Mie scattering model was used, for example, by Feng et al. (2013), Lu et al. (2015), and Romonosky et al. (2019).

The effective refractive index, m_{eff}, of an aerosol particle will be given by

$$m_{eff} = f m_{BC} + (1-f) m_{OC}, \tag{1}$$

where m_{BC} is a complex refractive index of BC, m_{OC} is a refractive index of OC, and f is a volume fraction of BC. The OC with a stronger absorption at the blue end of the spectrum than at the red end is called the BrC, and its refractive index at the blue end of spectrum will be denoted m_{BrC}.

3. Absorption Ångström Exponent

The absorption Ångström exponent (AAE) has been generally used to characterize the wavelength dependence of the slowly changing aerosol absorption. AAEs have been found useful in the classification of aerosols according to their origin, to distinguish between urban aerosol, biomass burning aerosols, or desert dust (e.g., Russell et al., 2010). We approximate the AAE between the two wavelengths λ_1 and λ_2 by

$$AAE\left(\frac{b_{abs\lambda_1}}{b_{abs\lambda_2}}\right) = -\frac{\ln\left(\frac{b_{abs\lambda_1}}{b_{abs\lambda_2}}\right)}{\ln\left(\frac{\lambda_1}{\lambda_2}\right)} = -\frac{\ln(b_{abs\lambda_1})-\ln(b_{abs\lambda_2})}{\ln(\lambda_1)-\ln(\lambda_2)}, \tag{2}$$

where λ_1 and λ_2 are the two wavelengths at which the AAE is calculated and the $b_{abs\lambda 1}$ and $b_{abs\lambda 2}$ are the absorption coefficients at the selected wavelengths λ_1 and λ_2. In this report, we will be working with the wavelengths at 405 and 781 nm determined by instruments we use (Gomez et al., 2018; Romonosky et al., 2019). Our phase space is defined by two variables: the AAE and a single-scattering albedo (SSA) at the wavelength 405 nm given by

$$SSA = \frac{b_{scat}}{b_{ext}}, \tag{3}$$

where b_{scat} and b_{ext} are the scattering and extinction coefficients.

Whenever we use the SSA or AAE without designating specifically which wavelengths are being used, it should be understood that we mean 405 nm for SSA and 405 nm and 781 nm for AAE.

From equation (2), it follows that

$$AAE\left(\frac{b_{abs\lambda_1}}{b_{abs\lambda_2}}\right) = 1 \tag{4}$$

if and only if

$$\ln\left(\frac{b_{abs\lambda_1}}{b_{abs\lambda_2}}\right) = -\ln\left(\frac{\lambda_1}{\lambda_2}\right), \tag{5}$$

which is approximately satisfied for small particles within the Rayleigh scattering regime where absorption varies with wavelength approximately as $1/\lambda$ and wherever else by chance equation (5) is satisfied. Thus, some of the earlier statements (e.g., Kirchstetter et al., 2004; Lack et al., 2008; Lack & Landridge, 2013; Lewis et al., 2008; Liu et al., 2015; Moosmuller et al., 2009; Russell et al., 2010) that AAE = 1 for BC or BC and OC mixture are generally not exact (Liu et al., 2018).

The definition of AAE by equation (2) allows us to derive an interesting relationship between AAE at some value $\frac{b_{abs\lambda_1}}{b_{abs\lambda_2}}$ and twice its value, $\frac{2b_{abs\lambda_1}}{b_{abs\lambda_2}}$. Following the definition of the AAE (equation (2)), we can write for the case when absorption is doubled at the wavelength λ_1

$$AAE\left(\frac{2b_{abs\lambda_1}}{b_{abs\lambda_2}}\right) = -\frac{\ln\left(\frac{2b_{abs\lambda_1}}{b_{abs\lambda_2}}\right)}{\ln\left(\frac{\lambda_1}{\lambda_2}\right)} = -\frac{\ln(2)}{\ln\left(\frac{\lambda_1}{\lambda_2}\right)} - \frac{\ln\left(\frac{b_{abs\lambda_1}}{b_{abs\lambda_2}}\right)}{\ln\left(\frac{\lambda_1}{\lambda_2}\right)}$$

and

$$AAE\left(\frac{2b_{abs\lambda_1}}{b_{abs\lambda_2}}\right) = AAE\left(\frac{b_{abs\lambda_1}}{b_{abs\lambda_2}}\right) + \frac{\ln(2)}{\ln\left(\frac{\lambda_2}{\lambda_1}\right)}. \tag{6}$$

If we select the wavelengths in such a way that their ratio $\lambda_1/\lambda_2 = 1/2$, for example 400 and 800 nm, we get

$$AAE\left(\frac{2b_{abs\lambda_1}}{b_{abs\lambda_2}}\right) = AAE\left(\frac{b_{abs\lambda_1}}{b_{abs\lambda_2}}\right) + 1 \tag{7a}$$

and

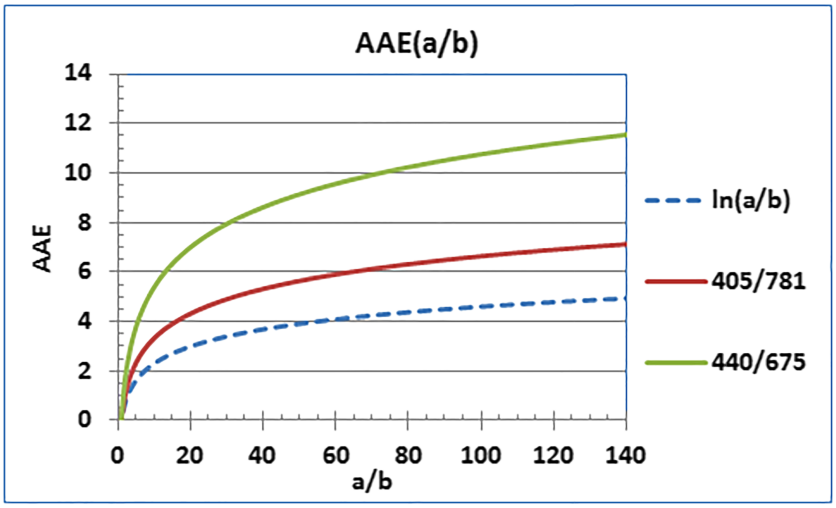

Figure 1. The absorption Ångström exponent (AAE) as a function of the ratio (a/b) of absorption at the blue end and the red end of the spectrum. The red curve is for the wavelengths of 405 and 781 nm, while the green curve for 440 and 675 nm. The dash curve shows just the ln(a/b). With each doubling of the ratio a/b, the red (405/781) curve increases by about 1.05 units of AAE (equation (8)).

$$AAE\left(\frac{2^n b_{abs\lambda_1}}{b_{abs\lambda_2}}\right) = AAE\left(\frac{b_{abs\lambda_1}}{b_{abs\lambda_2}}\right) + n, \qquad n = 1, 2, 3, ... \tag{7b}$$

Thus, in the case when absorption of aerosol particle at the shorter wavelength is doubled, and when the ratio of the wavelengths is exactly equal to 2, each doubling of absorption at the blue end increases the AAE value by one unit.

This (equation (7)) is an important new relationship derived just from the basic definition of the AAE approximation given by equation (2). For practical application, consider the case when, for example, AAE~6 is observed. Using equation (7), we can immediately deduce that the absorption of aerosol particle at the blue end is approximately 2^6 times stronger that absorption at the red end. In general, the derived relations (6–8) can be used to estimate the rate of absorption increase at the blue end of the spectrum from a measured value of AAE.

In our case, the wavelength ratio is not exactly 2, but 781/405 = 1.93. The increase of AAE with each doubling of the blue end absorption is then

$$AAE\left(\frac{2b_{abs\lambda_1}}{b_{abs\lambda_2}}\right) = AAE\left(\frac{b_{abs\lambda_1}}{b_{abs\lambda_2}}\right) + 1.05 \tag{8a}$$

$$AAE\left(\frac{2^n b_{abs\lambda_1}}{b_{abs\lambda_2}}\right) = AAE\left(\frac{b_{abs\lambda_1}}{b_{abs\lambda_2}}\right) + n^*1.05, \qquad n = 1, 2, 3, ... \tag{8b}$$

Sometimes, a different set of wavelengths are used to calculate AAE (Figure 1). The relationship between AAE at different sets of wavelengths can be written as

$$AAE(b_{abs\ \lambda 3}, b_{abs\ \lambda 4}) = AAE(b_{abs\ \lambda 1}, b_{abs\ \lambda 2}) \frac{\ln\left(\frac{\lambda 2}{\lambda 1}\right)\ln\left(\frac{b_{abs\ \lambda 3}}{b_{abs\ \lambda 4}}\right)}{\ln\left(\frac{\lambda 4}{\lambda 3}\right)\ln\left(\frac{b_{abs\ \lambda 1}}{b_{abs\ \lambda 2}}\right)}. \tag{9}$$

4. BC and AAE

One of the fundamental properties of BC (soot) is its refractive index. Since BC is produced by burning organic material, it is understandable that the refractive index of BC depends on how the BC was

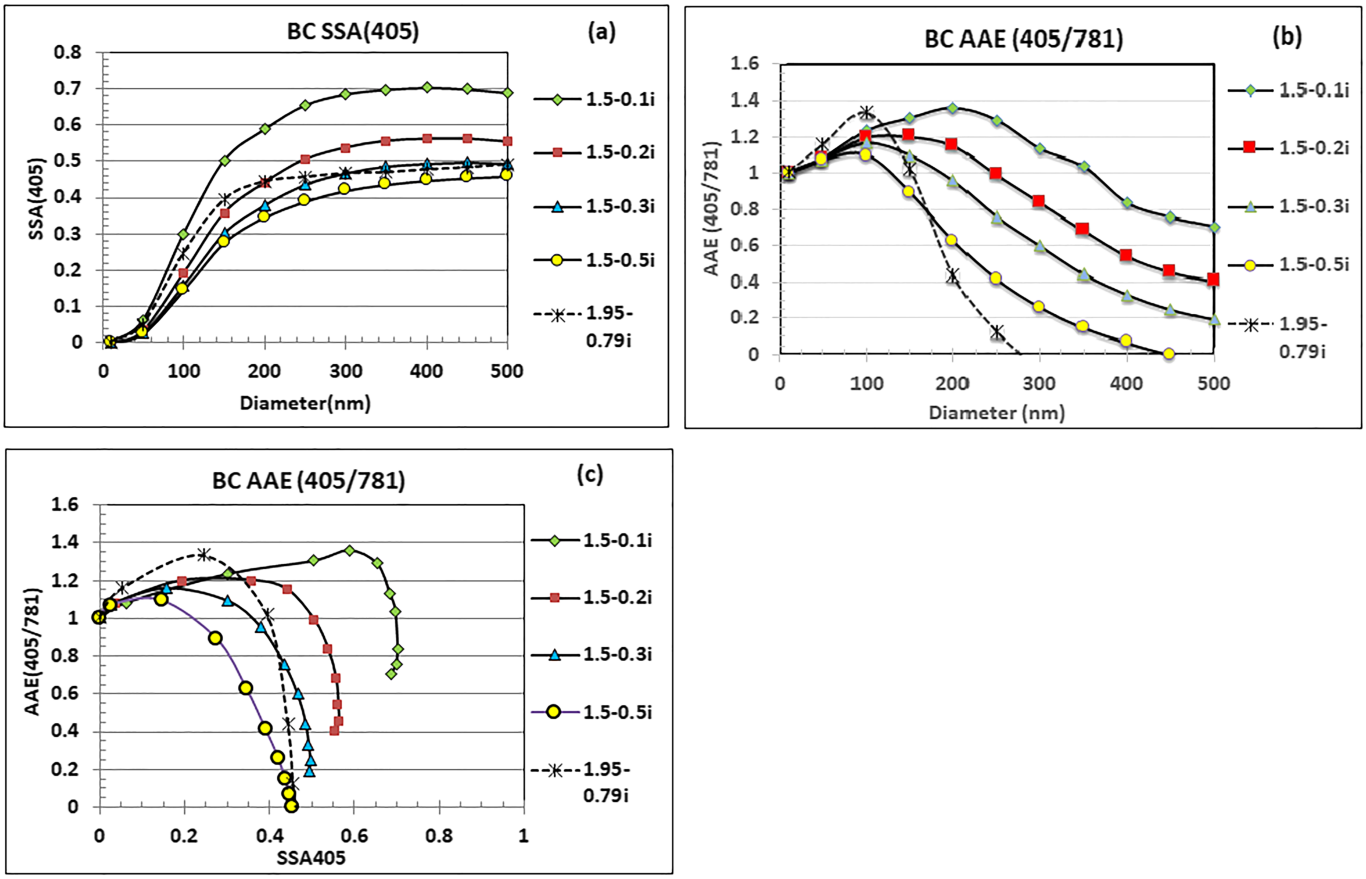

Figure 2. (a) Single-scattering albedo (SSA) of black carbon (BC) spherical particle at 405 nm wavelength as a function of particle diameter for different BC refractive indices. (b) The absorption Ångström exponent (AAE) as a function of particle diameter for different BC refractive indices. (c) The AAE, AAE(405/781), at the wavelengths of 405 and 781 nm as a function of the SSA(405) for specified BC refractive indices.

produced. It depends on the material being burned as well as on the process and environmental conditions during the burning. Thus, a wide range of values have been reported in the published literature. Although the BC refractive index m = 1.5–0.3i has been defined as a part of our Mie scattering model, we will consider BC refractive indices with the real part of 1.5 and imaginary parts between 0.1i and 0.5i. In addition, we also use the BC refractive index of 1.95–0.79i as recommended by Bond and Bergstrom (2007) and used in climate models.

The SSA at a given wavelength of a spherical homogeneous particle depends on the refractive index and on particle size. Extensive discussions of this have been recently given by Sorensen et al. (2019) and by Moosmuler and Sorensen (2018a, 2018b). Figure 2a shows SSA at 405 nm for several refractive indices of BC with diameters of the spherical particle from 10 to 500 nm. Figure 2b shows AAE(405/781) as a function of SSA(405) for the same BC particles.

In general, AAE = 1 for small particles within the Rayleigh limit, where absorption varies with wavelength as $1/\lambda$. Thus, AAE = 1 is a good approximation for small BC particles regardless of their refractive index and morphology. For particle sizes outside of the Rayleigh limit, AAE increases with increasing particle size (Figure 2b) until it reaches a constant or slowly varying value of SSA (Figure 2a). Then, AAE falls sharply (Figure 2b), passing through the value of AAE = 1 again at a specific size, which is different for each refractive index value. At this point, the ratio of absorption at the two considered wavelengths is equal to the reciprocal of the wavelength ratio. We note that for the considered range of refractive indices, AAE(405/781) for BC never reaches values over 1.4.

Thus, we set the upper limit on AAE(405/781) of BC to be

$$AAE_{BC}\left(\frac{405}{781}\right)\leq 1.4. \quad (10)$$

Our upper limit of BC AAE is the same as that that of Lack and Landridge (2013) of 1.1 ± 0.3. However, the lower AAE limit is a sensitive function of the refractive index and can be as low as zero (Figure 2b) for particle diameter ≤500 nm.

Given a real part of refractive index of BC, for each value of the imaginary part, there is a maximum value of SSA which a small spherical particle of that BC can reach. This provides an opportunity to estimate the imaginary part of the refractive index (assuming that the real part is known) of BC from the maximum SSA value (Figure 2b). For example, the samples used in laboratory measurements by Romonosky et al. (2019) and shown in their Figures 3 and 4, suggest by comparison with our Figure 2, the imaginary part of the refractive index close to 0.5i for BC, and close to 0.2i for nigrosin.

We also note that SSA and AAE properties of spherical particle with the refractive index of 1.95–0.79i are close to a particle with the index 1.5–0.3i (Figure 2). Consequently, only the SSA and AAE values for BC may not be able to distinguish between these pairs of refractive indices.

Several published papers suggested that the AAE = 1 for "pure" BC. It has been shown that this assumption may produce a considerable uncertainty in produced results (Lack & Landridge, 2013). Others proposed the AAE of BC to be <1 (e.g., Zhang et al., 2018). The larger BC particles (or aggregates of small particles) may have indeed the AAE values <1 depending on their diameter and refractive index (Figure 2b). Thus, both past claims are valid within specified particle size regions. Of course, as with each AAE value, the two wavelengths used need to be specified (405 and 781 nm in our case).

5. BC-OC in Internal Mixture

We now consider a mixture of BC with OC or water. We define OC as a material that does not absorb visible and near ultraviolet solar radiation. The goal is to determine the region of AAE(405/781) and SSA(405) phase space that can be occupied by this BC and OC mixture. In Figure 3, we show cases of several refractive indices of BC to explore across the range of possible AAE/SSA values. The first two points on each curve (Figure 3) are values of AAE and SSA for a diameter of a spherical particle of 10 and 50 nm. After that, the diameter increases in 50 nm steps up to 500 nm. The advantage of showing individual points is to retain the size related information, which would be lost if only smooth curves were presented.

A small amount of BC (1%) mixed in water ($m = 1.33$) or OC ($m = 1.46$) is characterized by a high value of the SSA(405) and by an AAE that approaches 1.4 for water (Figure 3a) and slightly over 1.6 for OC (Figure 3b). With an increasing concentration of BC, both the SSA and the AAE decrease. We note that the AAE, in the case of a mixture of BC and spectrally flat OC materials, never increases above about 1.63. This remains true even if we change the real part of refractive index of BC to 1.7 (Figure 3c) or change the imaginary part to 0.3 (Figure 3d), or if we adopt the refractive index of 1.95–0.79i. Thus, in agreement with earlier publications (Lack & Cappa, 2010; Romonosky et al., 2019; Zhang et al., 2018), and rounding to the higher one decimal place number, we conclude that the AAE(405/781) of a mixture of BC and spectrally flat organic material is limited by

$$AAE_{\frac{BC}{OC}}\left(\frac{405}{781}\right)\leq 1.7. \quad (11)$$

The same limit was deduced by Lack and Cappa (2010) using an aerosol particle model of a layered sphere with a BC core and a spherical shell of nonabsorbing or slightly absorbing material. In our work, this limit is a result of a simple Mie scattering by a homogeneous spherical particle and does not require a core-shell model.

In our model of internal mixture of BC and OC with spectrally flat refractive indices, the AAE values >1.7 cannot be reached. To explain AAE values larger than 1.7 with BC and organic material only (excluding mineral dust and other inorganic material), we need at least one of the materials present to have a higher imaginary part of the refractive index at the blue end of the solar spectrum than at the red end. An organic material with a higher imaginary part of the refractive index at the blue end

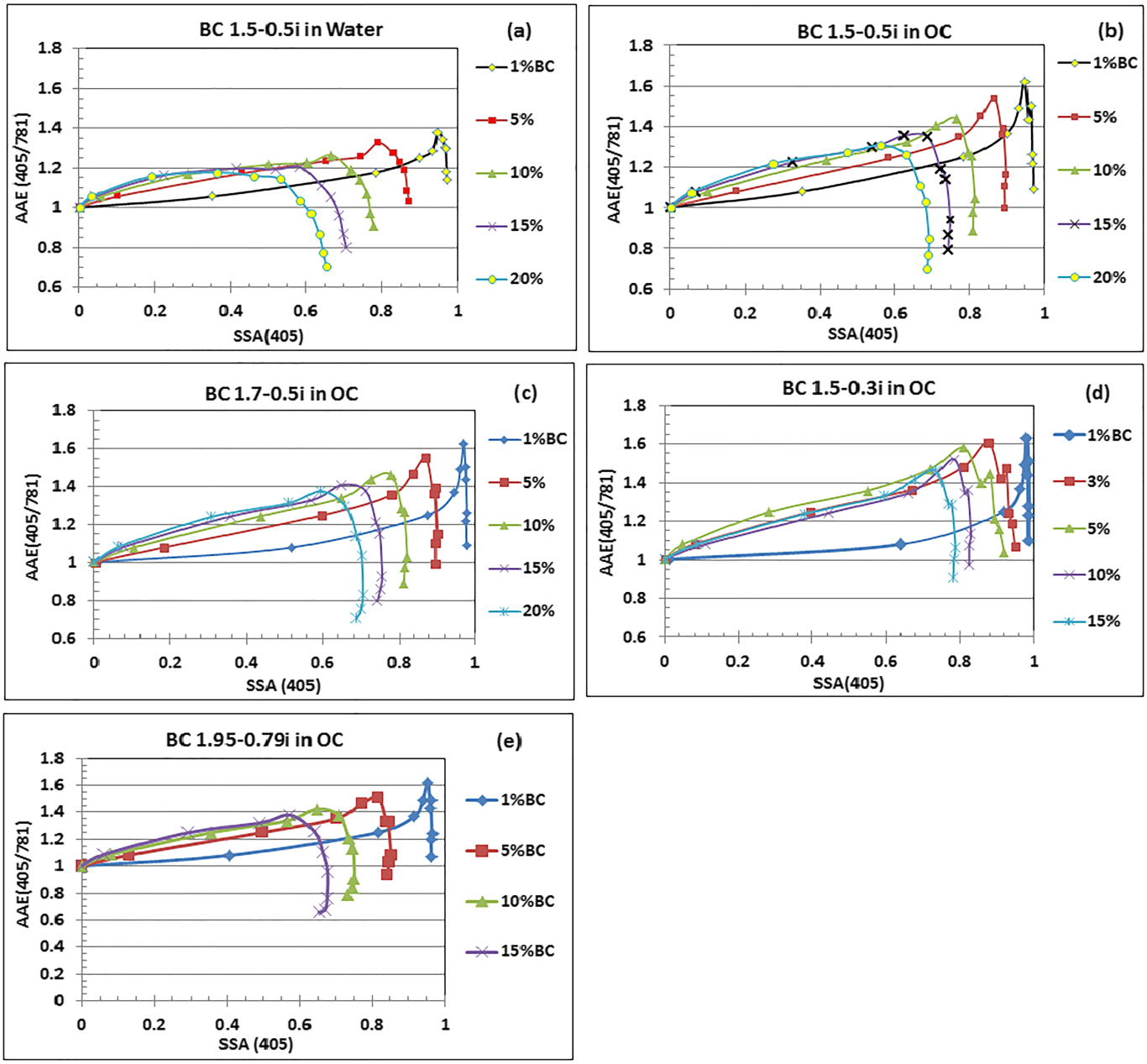

Figure 3. (a) absorption Ångström exponent (AAE) at wavelengths of 405 and 781 nm for different fractions of black carbon (BC) mixed with water as a function of a single scattering albedo (SSA) at 405 nm. Refractive index of BC is taken to be m_{BC} = 1.5–0.5i and that of water m = 1.33. The concentration of BC in water varies between 1% and 20%. An effective refractive index of the mixture is calculated by volume averaging the refractive indices of individual components. (b) Same as Panel a except for a mixture of BC and organic carbon (OC) with spectrally flat refractive index 1.46. (c) Same as Panel b except that the refractive index of BC is taken to be m_{BC} = 1.7–0.5i. (d) Same as Panel b except that the refractive index of BC is taken to be m_{BC} = 1.5–0.3i. (e) Same as Panel b except that the refractive index of BC is taken to be m_{BC} = 1.95–0.79i.

of the spectrum is known as BrC. Thus, for AAE values >1.7, BrC is a required component of the material mixture.

AAE generally increases with increasing diameter (Figure 3). Larger than some characteristic diameters, SSA changes only slightly or remains constant with increasing diameter, and the AAE value falls sharply. The value of the SSA at this downward turn characterizes a maximum value of the SSA which the corresponding mixture of BC and OC can achieve. Thus, each mixture of BC and OC can be characterized

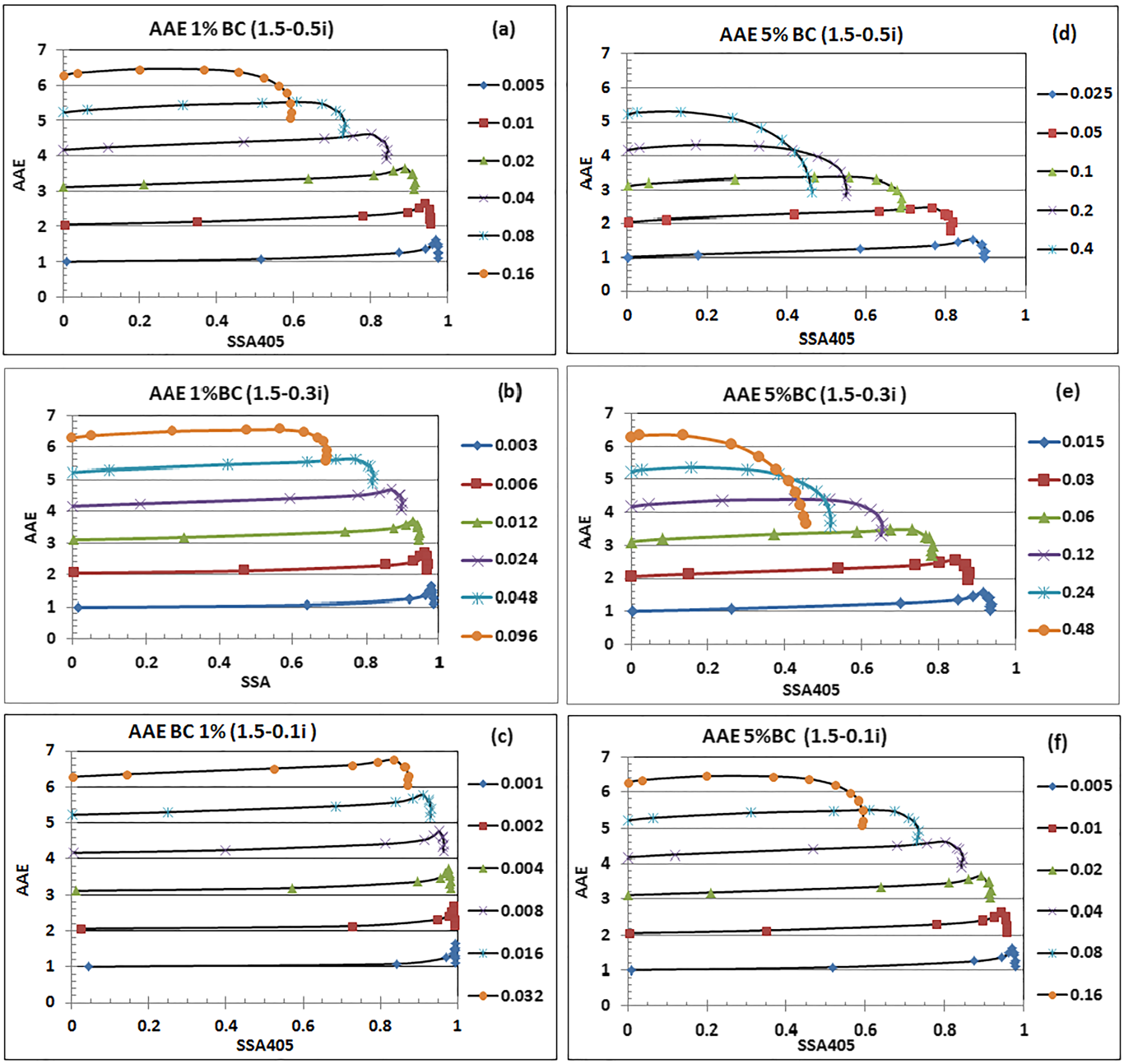

Figure 4. (a) The AAE(405/781) of a mixture of 1% of black carbon (BC) with a refractive index n (BC) = 1.5–0.5i and brown carbon (BrC)as a function of SSA(405) for the BrC real part of refractive index 1.46 and an imaginary part of an effective refractive index between 0.005i and 0.16i. (b) Same as in Panel 4a except for BC refractive index of 1.5–0.3i. (c) Same as in Panel 4a except for refractive index of 1.5–0.1i. (d) Same as in Panel 4a except for BC volume fraction of 5%. (e) Same as in Panel 4b except for BC volume fraction of 5%. (f) Same as in Panel 4c except for BC volume fraction of 5%. For each curve in each panel, the imaginary part of an effective refractive index of a sphere at 405 nm is doubled as shown in the right-hand column on each panel, while the refractive index at 781 nm is kept constant. The first two points on each curve correspond to a sphere with a diameter of 10 and 50 nm; after that, the diameter is increasing in 50 nm steps up to 500 nm. The individual curves in each panel are shifted upwards by 1.05 units of absorption Ångström exponent (AAE) according to the equation (8).

by a maximum value of the SSA it can reach. Therefore, the maximum SSA of a mixture can be used to estimate the percent of BC involved in the mixture (Figure 3), assuming the refractive index of BC is known.

6. BC-BrC Mixture

In field observations as well as in laboratory measurements, values of AAE >1.7 are frequently observed (Kirchstetter et al., 2004; Romonosky et al., 2019) and occasionally values of AAE ˃6 are reached (e.g.,

Chakrabarty et al., 2010; Liu, Scheuer, et al., 2014; Romonosky et al., 2019). These values AAE >1.7 cannot be explained without BrC. Here, we refer to BrC as an OC which has absorption at the blue end of the spectrum (in our case, at 405 nm) higher than the absorption at the red end (at 781 nm).

AAE(405/781) values for cases of BC refractive indices 1.5–0.5i, 1.5–0.3i, and 1.5–0.1i in 1% and 5% mixture with BrC are shown in Figure 4. The increasing BrC absorption is simulated by an increasing imaginary part of an effective refractive index at 405 nm. The right-hand column in each panel shows the chosen imaginary part of an effective refractive index of the mixture at 405 nm. The lowest imaginary part of an effective refractive index in each panel is given by the internal mixture of BC and OC only. After that, the imaginary part of an effective refractive index is doubled as the absorption of the organics at 405 nm is increased. With each doubling of the imaginary part of an effective refractive index, the AAE(405/781) increases by 1.05 (equation (8)). At the same time, the SSA at the short wavelength decreases. This decrease of the SSA is faster with higher BC fraction and with the higher absolute value of the imaginary part of effective refractive index (Figure 4).

The observed AAE(405/781) values of around 6 together with a SSA(405) of over 0.9 require special consideration. With the BC refractive index of 1.5–0.5i, when we reach AAE around 6, the SSA has already decreased to well below 0.55 (Figure 4a the top curve). It is clear that this BC refractive index (1.5–0.5i) cannot explain the observed high values of AAE (AAE > 6), and at the same time, the high values of SSA (SSA > 0.9). In this case, we need BC with a much smaller imaginary part of refractive index. Figure 4c shows the case of 1% BC with a refractive index of n = 1.5–0.1i. A high value of AAE~6 is reached while the SSA remains around 0.9. Thus, the observed high values of AAE > 6 require, within the range of refractive indices considered, a small amount of BC (≤1%) with a small imaginary part of BC refractive index, not larger than 0.1.

In general, the pair of values of the SSA(405) and the AAE(405/781) (Figure 4) determines the imaginary part of the effective refractive index of an internal mixture of BC and BrC (right hand column in each panel of Figure 4). Using the deduced imaginary part of an effective refractive index and the mixing rule (equation (1)), the imaginary part of the refractive index of BrC can be calculated. When there are more than one possible solutions for a given pair of the SSA and the AAE (e.g., Figures 4a and 4f), they lead to the same (or very close to each other) values of the imaginary part of refractive index of BrC (Table 1).

7. Biomass Burning Ambient Fires

There have been many laboratory measurements and field data analysis leading to the estimate of an imaginary part of refractive index of BrC. The deduced range spans from 0.01 to about 0.2 at short wavelength (Kirchstetter et al., 2004; Alexander et al., 2008; Wang et al., 2014; Saleh et al., 2013, 2014; 2018; Cappa et al., 2019). We use the presented Mie scattering model to deduce an imaginary part of refractive index of BrC. The list of southwestern fires (Romonosky et al., 2019) together with the two Atmospheric Radiation Monitoring (ARM) field observations (Green Ocean Amazon [GOAmazon] and Layered Atlantic Smoke Interactions with Clouds [LASIC]) are provided in Table 1.

To deduce the parameters of internal mixtures from their mean values of AAE(405/781) and SSA(405), we divide the mixtures into different bands according to the AAE values. We already know that for AAE <1.7, we do not need any BrC to obtain an agreement between the observations and model results. Let us consider first the AAE band between 2.7 and 3.7. There is only one biomass burning plume (Whitewater Baldy; WWB) that has a mean value of the AAE within this band (Table 1). To approximate the maximum value of SSA for each curve in Figure 4, we average SSAs for particle diameter 300 ≤ d ≤ 500 nm (the last five points on each curve in Figure 4). The same procedure is followed for AAE values between 1.7 and 2.7.

The model estimated maximum SSA for a selected set of BC refractive indices (1.5–0.5i, 1.5–0.3i, and 1.5–0.1i) and selected set of BC volume fractions (1, 3, and 5%) is shown in Figure 5. The observed mean SSA of the considered ambient biomass burning fire can be matched with one of the modeled SSA. This determines the effective refractive index of the aerosol particles (the second row of panels in Figure 5). Using the mixing rule (equation (1)), the imaginary part of refractive index of BrC is now obtained (the third line of panels in Figure 5).

Table 1
The List of U.S. Southwestern Fires Plus GOAmazon and LASIC

biomass burning (BB) Fire	SSA	*SD*	AAE	*SD*	*m* (BC)	%BC	Im (m_{eff})	Im (m_{BrC})
Whitewater Baldy	0.911	0.007	3.30	0.35	1.5–0.3i	1.8%	0.021	0.016
					1.95–0.79i	0.6%	0.019	0.015
San Antonio	0.905	0.011	2.38	0.89	1.5–0.3i	3.7%	0.022	0.011
					1.95–0.79i	1.4%	0.022	0.011
Las Conchas 1	0.913	0.018	2.26	0.46	1.5–0.3i	3.3%	0.020 0.020	0.010
					1.95–0.79i	1.3%		0.010
Las Conchas 2	0.894	0.016	1.51	0.18	1.5–0.3i	5%	0.015 (+30%)	≤0.005
Buzzard	0.912	0.012	1.44	0.39	1.5–0.3i	5%	0.015 (+30%)	≤0.005
Ute Park	0.912	0.013	1.42	0.75	1.5–0.3i	5%	0.015 (+30%)	≤0.005
GOAmazon	0.867	0.007	1.27	0.17	1.5–0.3i	10%		N/A
					1.95–0.79i	5%		
LASIC	0.79	0.03	1.04	0.10	1.5–0.3i	15%		N/A
					1.95–0.79i	7%		

Note. The individual columns represent in order the name of the biomass burning fire, SSA at 405 nm, standard deviation of the measured SSA, Ångström Absorption Exponent at 405/781 nm wavelengths, AAE standard deviation, assumed value of the refractive index of BC, fraction of BC (in %) present, imaginary part of effective refractive index of aerosol particle, Im (m_{eff}), and imaginary part of refractive index of brown carbon, Im (BrC). Two very different refractive indices of BC (1.5–0.3i and 1.95–0.79i) are considered leading to an almost identical imaginary part of BrC refractive index. The decimal places in %BC were obtained by interpolation between the integer values. The Im (m_{eff}) of the Las Conchas 2, Buzzard, and Ute Park was increased by 30% before estimation of the upper limit on Im (m_{BrC}). The values shown in Columns 2 to 5 are from in situ optical measurements of smokes. The values of BC refractive index, m (BC), are assumed. The percent of BC and the imaginary part of refractive index of mixture Im (m_{eff}) are deduced from the Mie scattering model (from graphs similar to those shown in Figure 4). Finally, the imaginary part of the BrC refractive index (Im (m_{BrC}) at 405 nm is calculated using the volume averaging mixing rule.
Abbreviations: AAE, absorption Ångström exponent; BC, black carbon; BrC, Brown carbon; GOAmazon, Green Ocean Amazon; LASIC, Layered Atlantic Smoke Interactions with Clouds; SSA, single-scattering albedo.
biomass burning (BB).

A large portion of biomass burning fires are smoldering fires. Thus, the imaginary part of refractive index of BC is expected to be relatively low. We use the BC refractive index of 1.5–0.3i for the following analysis of ambient biomass burning fires. This relatively low imaginary part is close to the imaginary part of the BC refractive index of 0.2i deduced from observation of Amazonian plumes (Schmid et al., 2009) or laboratory-produced methane soot with an imaginary part of refractive index of 0.3i (Habib & Vervisch, 1988).

There is not a unique value of the BC refractive index that should be used for all biomass burning fires. The power of BC to absorb solar radiation, characterized by the imaginary part of its refractive index, depends on the material being burned and on the form of burning. When carbonization is not complete, the imaginary part of refractive index of BC is lower than the value expected for fully carbonized BC.

The AAE(405/781) and SSA(405) values of several southwestern fires (Las Conchas, WWB, Buzzard, Ute Park, and San Antonio) are shown in Figure 6. Details concerning these fires can be found in Romonosky et al. (2019). The Las Conchas fire data were divided into two groups according to a high or low AAE value. In addition to biomass burning fires, we consider the results of two major Department of Energy (DOE) Atmospheric Radiation Measurements Climate Research Facility field programs, namely GOAmazon (Martin et al., 2017) and the LASIC (Zuidema et al., 2018). GOAmazon data were collected at ARM's field site in Manacapuru, Amazon, during the 2014 dry biomass burning season. The LASIC data sampled African biomass burning plumes that have aged over a timescale of a few weeks. The southwestern plumes were observed within a few hours after the smoke emission.

The mean values of the SSA of the southwestern fires are clustered near SSA(405) = 0.9 ± 0.1. However, their AAE(405/781) varies significantly with mean values between 1.4 and 3.3, indicating different amounts or different properties of BrC present.

The two field programs (GOAmazon and LASIC) show lower SSAs than the U.S. southwestern fires. The lowest value of the SSA = 0.79 is observed for the LASIC campaign. Here the African biomass burning smoke is analyzed a few weeks after emission in the middle of southern Atlantic at Ascension Island (Zuidema et al., 2018). During the transport, aging, and modification, the OC (including BrC) can be removed, which leads to a higher fraction of BC, lower SSA, and lower AAE values (Figure 6).

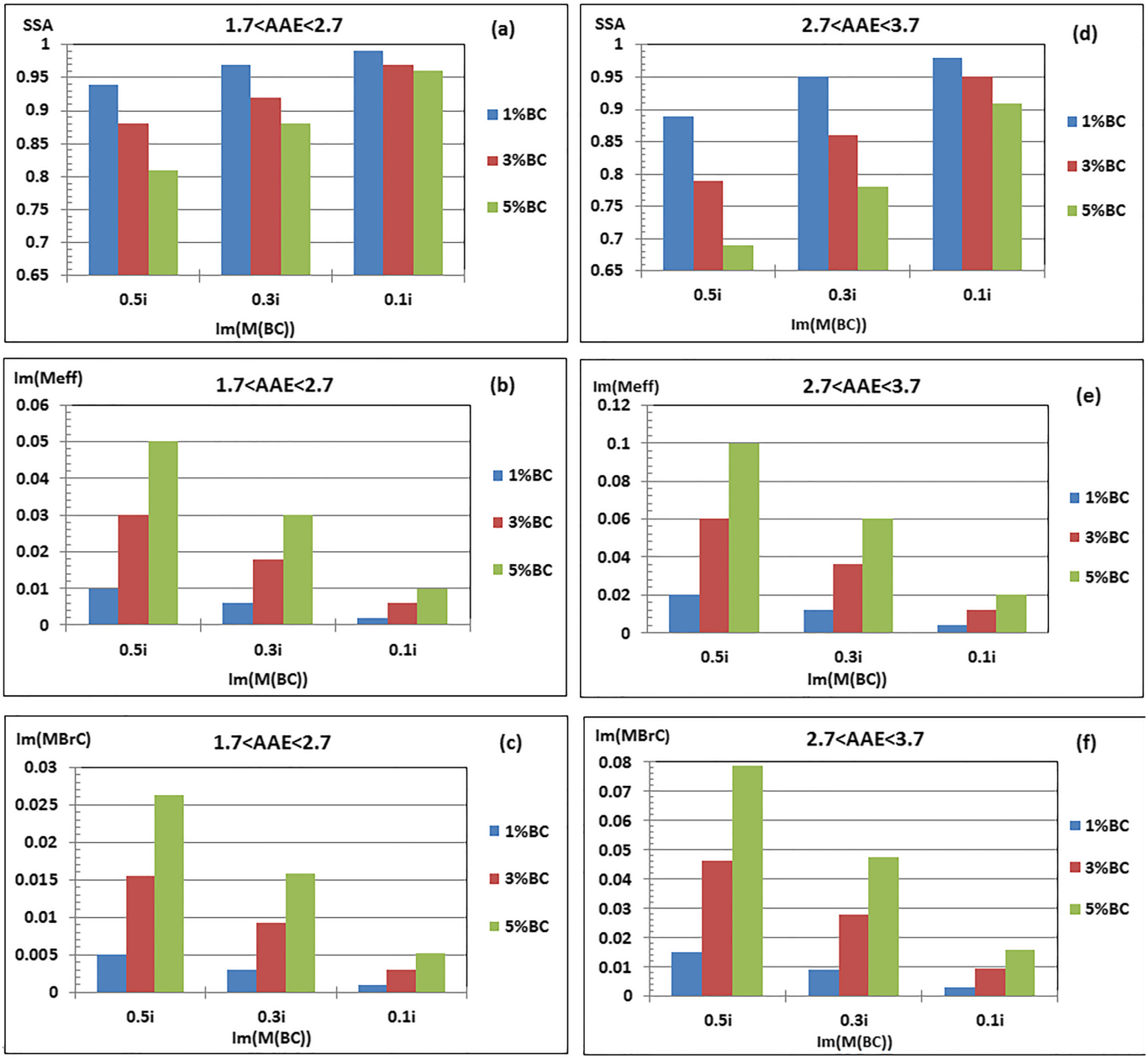

Figure 5. The model results for two groups of brown carbon (BrC) with the AAE(405/781) between 1.7 and 2.7 (Panels a, b. and c), and absorption Ångström exponent (AAE) between 2.7 and 3.7 (Panels d, e, and f). (a) The SSA(405) for three values of imaginary part of refractive index of BC (0.1i, 0.3i, and 0.5i) and for three fractions of BC within an aerosol particle (1%, 3%, and 5%). (b) The imaginary part of an effective refractive index of the appropriate internal mixture. (c) The deduced imaginary part of the refractive index of the BrC for each considered mixture. (d, e, and f) The same as a, b, and c, except for the AAE from 2.7 to 3.7.

The three plumes with mean AAE >1.7 (San Antonio, Las Conchas 1, and WWB) indicate the presence of the BrC. Following the procedure described, we estimate a fraction of BC in the mixture using the observed range of the AAE(405/781) and the mean value of the SSA(405). This is followed by determination of the imaginary part of an effective refractive index of a mixture and calculation of an imaginary part of a complex refractive index of BrC. The results are summarized in the last column of Table 1. The LASIC data taken in the middle of south Atlantic might contain some sea salt with much different chemical composition and radiative properties (Ma et al., 2008; Winter & Chylek, 1997). However, most of the sea salt was likely eliminated by considering aerosol particles below 1 μm diameter.

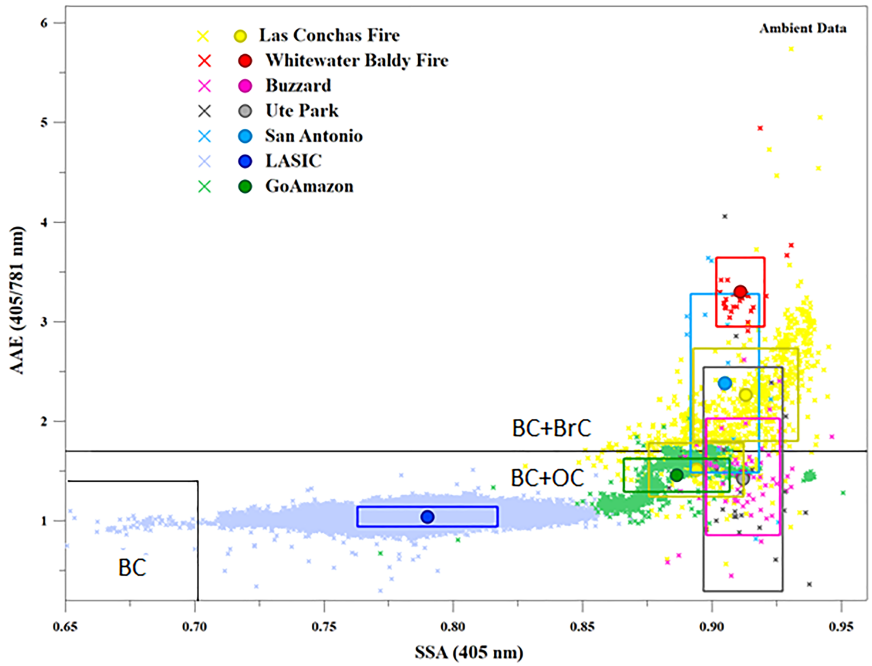

Figure 6. AAE(405/781) and SSA(405) data for several ambient southwestern fires and from the DOE GOAmazon and LASIC field campaigns. The points denote individual observations, circles are the means, and the colored boxes designate regions of the mean ± 1 standard deviation. The Las Conchas fire data are split into two parts with mean value of absorption Ångström exponent (AAE) ≤ 1.7 and AAE > 1.7. A horizontal line at AAE = 1.7 divides the AAE/SSA space into regions where BrC is (above this line) or is not (below this line) required.

The three datasets (Ute Park, Buzzard and Las Conchas 2) do not require any BrC to explain their SSA and AAE values. This does not, however, preclude the presence of some BrC. To estimate an absorbance of a potentially present BrC, we have increased the imaginary part of an effective refractive index of internal mixture, Im (m_{eff}), by 30% to estimate an imaginary part of refractive index of potentially present BrC (last column in Table 1).

The deduced imaginary part of the refractive index of BrC in ambient biomass burning fires (Table 1) is at the lower end of previously reported data (e.g., Wang et al., 2014). However it is consistent with results reported by Chakrabarty et al. (2010), Lack et al. (2012), Feng et al. (2013), and Cappa et al. (2019). The imaginary part of an effective refractive index of aerosol particle, Im (meff) in Table 1, from 0.015 to 0.022, is also comparable to the range of the imaginary part of aerosol particle refractive indices, from 0.010 to 0.021, derived from AERONET data for biomass burning regions of Africa and South America (Dubovik et al., 2002).

After finishing our analysis using BC refractive index of 1.5–0.3i, we repeated the whole process now using the refractive index of 1.95–0.79i. The final results, the imaginary part of refractive index of BrC, was found to be almost identical to those deduced using the BC index of 1.5–0.3i (Table 1). This can be understood from the equation for the imaginary part of BrC refractive index

$$Im(m_{BrC}) = \frac{Im(m_{eff}) - fIm(m_{BC})}{1-f}. \quad (12)$$

The volume fraction of BC, f, is in our cases usually <<1. Therefore, for a given m_{eff}, as long as the product $fIm(m_{BC})$ remains about a constant, the $Im(m_{BrC})$ will change very little with changing imaginary part of refractive index of BC. It is only the total strength of BC absorption characterized by the product of the imaginary part of refractive index and volume fraction of BC which enters equation (12). As long as this product remains constant, the $Im(m_{BrC})$ will change very little. To determine the imaginary part of BC refractive index, we would need an independent measurement of the BC fraction present in biomass burning aerosol particles.

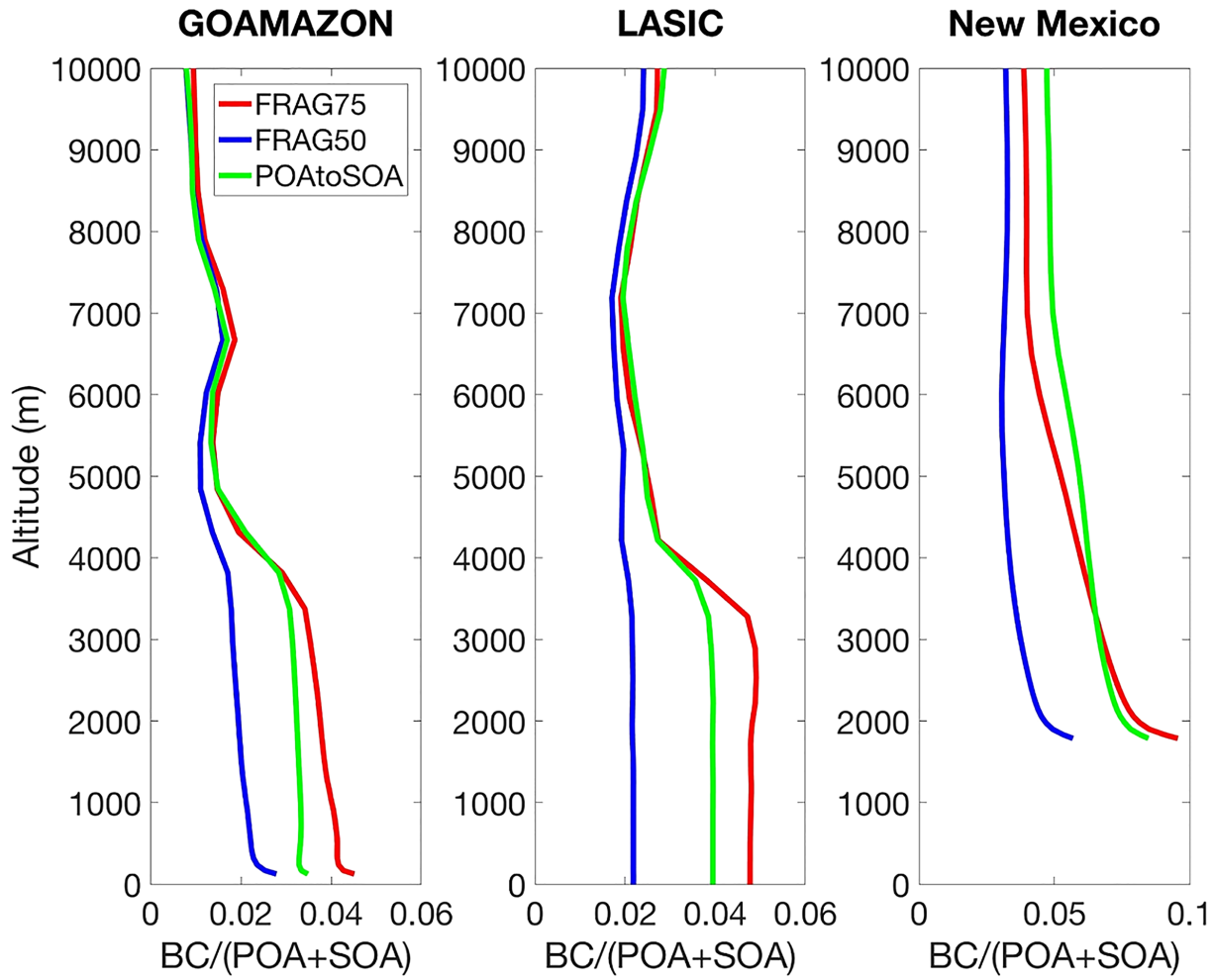

Figure 7. Exascale Earth System Model-simulated vertical profiles of ratios of BC to OA for three different SOA sensitivity simulations around the Amazon (3.2°S, 60.6°W) and LASIC (8.0°S, 14.5°W) sites and the mean over the state of New Mexico (32.1-37°N, 103.2-109.0°W).

Our result for the BrC refractive index assumes that all the organic mass is the BrC. This is similar to work of Lu et al. (2015). On the other hand, Feng et al. (2013) assumes that only 66% of the total OC mass is BrC. To compare our results with those of Feng et al., our imaginary part of refractive index of BrC has to be divided by 0.66.

A new DOE climate model, Exascale Earth System Model (E3SM), not yet perfectly tuned (Golaz et al., 2019; Rasch et al., 2019), was recently modified for major aerosol species production and transport including BC, primary organic aerosol (POA), and secondary organic aerosol (SOA). The ratios of vertical profiles of BC to OA (sum of POA and SOA) from the Amazon (September), LASIC (August–September), and southwestern fires in New Mexico (May–June) are provided in Figure 7. E3SM sensitivity simulations were conducted varying multigenerational chemistry of SOA precursors emitted from urban and biomass-burning sources. FRAG75 (75% fragmentation) and FRAG50 (50% fragmentation) represent simulations varying the fragmentation to functionalization branching ratio during aging of SOA precursors, as described in Shrivastava et al. (2015). POA to SOA represent a simplified treatment of POA that is converted to SOA assuming a 1-day aging timescale.

8. Relations Between Ambient Fires Parameters

Till now, we have considered each of the ambient fire individually without any relation to other fires. Now we look for similarities between all the considered biomass burning fires. Most of the fires considered were smoldering fires. Figure 8a shows a relationship between the SSA(405) and the percent of BC in

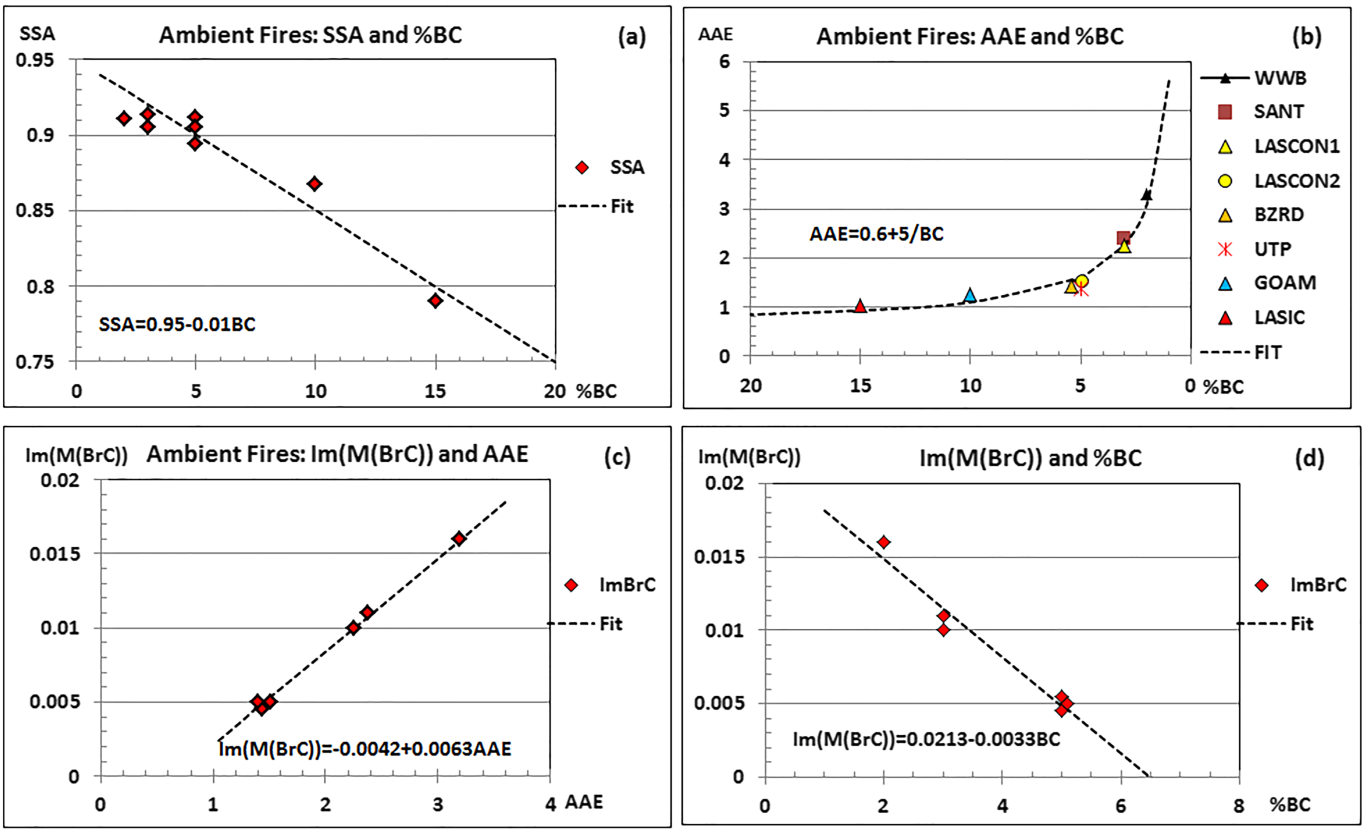

Figure 8. Our analysis of several ambient biomass burning fires suggests definite relationships between the variables. (a) A single-scattering albedo (SSA) decreases with the increasing amount of black carbon (BC) in the mixture. (b) The absorption Ångström exponent (AAE) decreases hyperbolically with an increasing fraction of BC. (c) Imaginary part of the brown carbon (BrC) refractive index increases linearly with the AAE of the plume. (d) The imaginary part of the BrC refractive index decreases linearly with an increasing fraction of BC. The dashed lines in all panels represent approximate fits to experimental data. All derived relationships between the variables are expected to be valid for predominantly smoldering biomass burning fires.

biomass burning aerosol particles. As expected, we observe that with increasing fraction of highly absorbing BC, the SSA decreases. The decrease is approximately linear with the relation between the SSA and BC given by

$$SSA = 0.942 - 0.009BC, \tag{13}$$

where BC is a volume fraction of BC in percent. A similar linear relationship between the BC and SSA has been reported earlier by Pokhrel et al. (2016) by analysis of laboratory FLAME-4 measurements with quantitatively similar coefficients (0.91 instead of 0.942 and 0.0087 instead of 0.009).

Next we look for a relationship between the AAE(405/781) and the volume fraction of BC (Figure 8b). All the points representing the observed fires form a curve approximated by the equation

$$AAE = 0.6 + \frac{5}{BC}, \tag{14}$$

where again the BC stands for a BC volume fraction in percent.

Equations (13) and (14) provide "rather surprising but useful results" (Pokhrel et al., 2016), suggesting that the knowledge of the fraction of BC in the mixture allows us to estimate the SSA and the AAE. In our case, we have derived appropriate relations (13 and 14) from the ambient plumes fire observations while Pokhrel et al. (2016) derived similar relations from analysis of laboratory data.

The relation between the imaginary part of the BrC refractive index and the observed mean AAE(405/781) of the ambient fire data is given by

$$Im(M(BrC)) = -0.0042 + 0.0063AAE \tag{15}$$

or as a function of BC

$$Im(M(BrC)) = 0.0213 - 0.0033BC. \tag{16}$$

Thus, the imaginary part of BrC refractive index increases approximately linearly with the observed AAE and decreases linearly with increasing fraction of BC. In another words, the imaginary part of BrC refractive index is anticorrelated to the volume fraction of BC present. This supports the idea that both the BC and BrC are produced by the same biomass burning mechanism with the BrC turning to the BC with increasing temperature of the flame, as suggested by Saleh et al. (2014, 2018).

The fact that these relations (equations (13) to (16)) were derived in our case from the SSA and AAE assigned to individual ambient fires based on a simple Mie scattering model suggests that the model works as expected describing correctly, even though approximately, the basic relationship between the individual smoke variables. AAE can be useful to estimate the fraction of BC in aerosol particle (Figure 8b). SSA can be useful for estimating fractions of BC (Figure 8a). Both AAE and BC fractions can be used to estimate the imaginary part of BrC refractive index in ambient biomass burning fires (Figures 8c and 8d).

9. Laboratory Measurements

In our laboratory experiment, we performed 21 individual burns of Russian olive wood using the approach described by Romonosky et al. (2019). The absorption and scattering coefficients were measured with a photoacoustic soot spectrometer (Droplet Measurement Technologies PASS-3). Absorption and scattering data are reported at 1-min resolution, represented by individual data points in Figure 8 a. Each burn includes 20–40 min of data; individual burns are coded by different colors. Fuel for the burns was about 0.50 g of dried Russian olive branches ground with an electric coffee blade grinder and was comprised of pieces ranging from fine dust to 2-cm long "sticks" approximately 1–3 mm diameter. Burns were ignited with an electric resistance heater held over the fuel for 10 s. Aerosols emitted from the burns were sampled through a cyclone (URG-2000-30EHB) which removes aerosols greater than 1 micron in diameter.

Although the controlled conditions were the same for all the burns, the AAE/SSA data are scattered across a wide range of these two variables. This suggests that the conditions of burning not controlled in the experiments varied significantly, as discussed in detail by Romonosky et (2019). For example, at low ignition temperatures, the fire can start as smoldering and upon heating transition to flaming at the end. At the other limit at high ignition temperatures, the fire can start of as flaming and then transition to smoldering as it runs out of fuel. We are unable to control these environmental variables or the airflow rate. Our data does sample the complete SSA and AAE spectrum as shown in Figure 9a. From the 21 burns, 10 had mean AAE below 1.7 and 11 had AAE above 1.7. Thus, about 50% of experiments produced plume that contained BrC, while in the other 50%, the BC and OC were sufficient to explain the observed values.

The curves of ambient plumes and laboratory biomass burnings in the AAE/SSA space are not identical (Figure 9b). We have

$$AAE = -0.23 + (1 - 1.10 * SSA)^{-0.12} \tag{17}$$

for ambient plumes and

$$AAE = -0.27 + (1 - 1.06 * SSA)^{-0.43} \tag{18}$$

for laboratory data. While additive and multiplicative coefficients are not too different, it is the exponent of 0.12 and 0.43 that makes the difference between the ambient and laboratory samples.

In general, the ambient plumes' AAE is shifted towards the higher values of SSA compared to laboratory experiment. A shift in the direction of a higher SSA means less absorption. Since the BC is not removed from the aerosol particles, possible causes of lower absorption include the BC particles that grow by coagulation and collapse to larger sizes with lower specific absorption per gram and/or aging mixes BC with organics

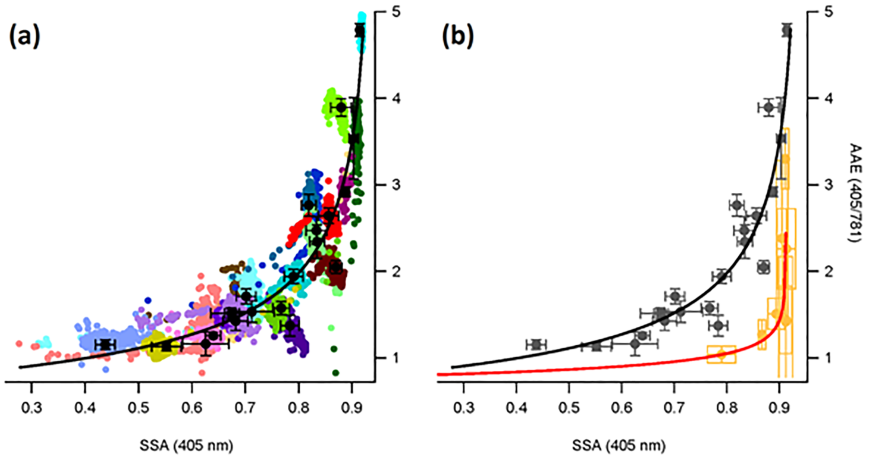

Figure 9. (a) Results of 21 laboratory biomass burning experiments. Each experiment leads to 20–40 min of data distinguished by different colors shown in panel. (b) The laboratory data (black) and ambient plume data (red) are located on different curves in the AAE/SSA space.

in the plume and other constituents in the ambient air. In the case of our laboratory burning experiments, there is a short time for coagulation and collapse and photochemical oxidation, while in the case of ambient fires, there are hours to days available for these processes to take place.

Furthermore, in laboratory experiments, the measurements are done within a few minutes after the burning. The structure of BC is likely highly nonspherical, and more complex models of optical properties of composite particles will be required.

10. Direct Radiative Forcing by Biomass Burning Aerosols

The aerosol direct radiative forcing by absorbing aerosols can be estimated from the expression derived by Chylek and Wong from a thin atmosphere limit of a radiative transfer equation (Chylek et al., 1995; Chylek & Coakley, 1974; Chylek & Wong, 1995; Coakley & Chylek, 1975; Hobbs et al., 1997)

$$\Delta F = -\frac{S_o}{4} T_{atm}^2 (1-N)\left[2(1-a)^2 \beta \tau_{sc} - 4a\tau_{abs}\right] \tag{19}$$

or from its later slight modification (Bond & Bergstrom, 2007). Here, ΔF is a change of radiative flux at the top of the atmosphere, S_o is a solar constant, T_{atm} is an average atmospheric transmission for solar radiation, N is the mean cloudiness, a is the surface albedo, and β is the upward scattering fraction. The τ_{sc} and τ_{abs} are the scattering and absorption optical depths.

As long as

$$K = \frac{2(1-a)^2 \beta}{4a} \geq \frac{\tau_{abs}}{\tau_{sc}}, \tag{20}$$

the direct radiative forcing will be negative and aerosol will cool the atmosphere. Within the Mie scattering model, the ratio of optical depths τ_{abs}/τ_{sc} can be calculated for a given BC refractive index, BC volume fraction, and an observed AAE value of the biomass burning plume.

Figure 10 shows the K values (defined by equation (20)) as a function of the surface albedo. The up-scattering fraction is taken as $\beta = 0.20$ (Chylek & Wong, 1995). The ratio τ_{abs}/τ_{sc} is calculated for three AAE bands, for AAE < 1.7, 1.7 < AAE < 2.7, and 2.7 < AAE < 3.7, and averaged over the aerosol particle diameter between 300 and 500 nm. The warming occurs to the right of the solid black curve. As can be seen (Figure 10), the aerosols without BrC (AAE < 1.7) will warm the atmosphere over surface albedo $a > 0.6$, which is limited to surfaces covered by ice and snow. The biomass burning plumes with the 1.7 < AAE <2.7 will warm over the surface with albedo $a > 0.45$, and plumes with 2.7 < AAE < 3.7 will warm the atmosphere over the

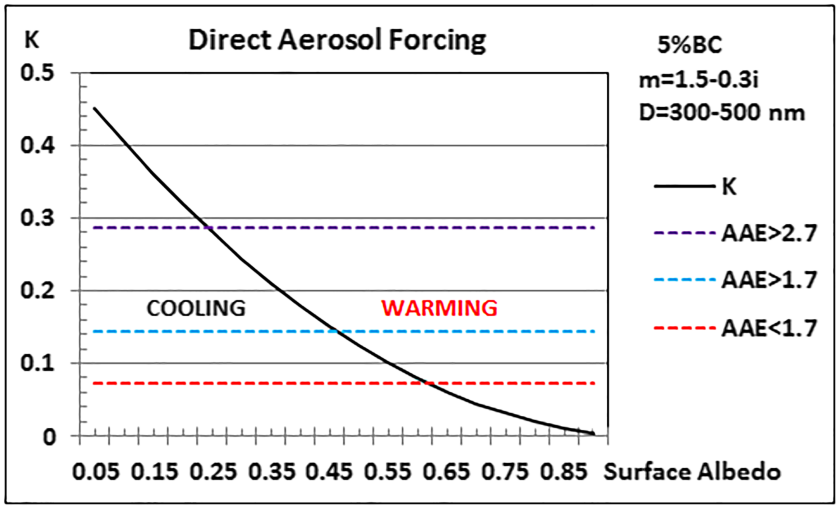

Figure 10. A direct brown carbon radiative forcing causing a cooling or a warming of the atmosphere depending on the surface albedo and on the absorption Ångström exponent (AAE) of the biomass burning plume. The calculation shown is for the blue end of the solar spectrum at the wavelength of 405 nm, average for particle diameters from 300 to 500 nm, for the BC refractive index of 1.5–0.3i and the BC volume fraction of 5%. K stands for expression defined by equation (20). Other choices of parameters will change the K-curve only slightly. The warming occurs on the right hand side of the K curve, and cooling on the left-hand side. The colored dash lines represent the AAE smaller than 1.7 (red), between 1.7 and 2.7 (blue), and between 2.7 and 3.7 (black). Although plumes with the AAE > 2.7 will cause warming over surfaces with a > 0.25, such plumes are rare.

surface with albedo a > 0.25. Thus, to get a warming effect over a significant part of Earth surface, we need biomass burning plumes with AAE > 2.7, which are values not observed frequently in ambient fires. These limits on the surface albedo will change slightly when the up-scattering fraction β is changed between the estimated values of 0.16–0.26 (Bond & Bergstrom, 2007; Chakrabarty et al., 2016; Chylek & Wong, 1995; Hobbs et al., 1997). A similar discussion showing the dependence of the warming/cooling on the surface albedo was presented in Chylek and Coakley (1974).

Considering that the biomass burning ambient plumes observed with AAE > 2.7 are infrequent even within a few hours after the emission, and relatively short BrC lifetime (of the order of less than a day), the global long-term effect of BrC from large fire plumes with properties similar to those we have analyzed on climate is expected to be rather limited. In addition, our radiative forcing estimate is at the 405-nm wavelength, which represents the maximum forcing compared to other wavelengths of solar spectrum. At the longer wavelengths, the effect of BrC will be weaker and will diminish towards the red end of solar spectrum.

The BrC effect may have some direct radiative climate-related significance in geographically limited regions where the biomass burning is steady, like in regions where wooden stoves are used daily for cooking or heating purposes (Ahmed et al., 2018; Feng et al., 2013). The cooling/warming regime may also change by considering the semidirect and indirect aerosol effects (e.g., Jacobson, 2014), which are not considered in this study. The global direct biomass burning climate effects might also become significant in the case of disastrous continent-wide fires.

11. Conclusion and Summary

We used a simple model of biomass burning aerosol consisting of homogeneous spherical particles and volume mixing of refractive indices. This avoids introducing additional parameters needed for more complicated models that are often difficult to measure. This also simplifies climate model parameterizations of biomass burning aerosols.

We have shown that several known limits on the AAE values follow directly from the Mie scattering by spherical particles without any requirement of a more complicated structure, like a core-shell model. The mixture of BC and OC is limited by AAE ≤ 1.7. Any value of AAE above this limit requires the presence of BrC.

Similarly, we find that AAE limit for pure BC is AAE $\leq$ 1.4. The frequently used assumption of AAE = 1 is generally valid for small aerosol particles in Rayleigh scattering limit.

We have derived quantitative relations (equations (13)–(16)) between the values of the AAE, BC fraction, and the imaginary part of refractive index of BrC, using ambient plumes field observations. In the case when the ratio of the two wavelengths used in an approximation of AAE (equation (2)) is equal to 2, the AAE increases by one unit with each doubling of the imaginary part of an effective refractive index of a particle (equation (7)).

The current spread of reported values of the imaginary part of BrC refractive index ranges from 0.01 to about 0.20. The values we obtain using Mie scattering model are close to the lower edge of published range consistent with studies of BrC effects by Chakrabarty et al. (2010), Lack et al. (2012), Feng et al. (2013), and Cappa et al. (2019). We also show that aged ambient plumes have larger SSA for a given value of AAE than laboratory experiments (Figure 9).

Finally, our study reduces the range of potential global direct radiative forcing by BrC from large fire episodes and shifts it to lower impacts. Based on our results, positive climate forcing due to BrC is rather limited due to its low imaginary part of refractive index, short lifetime, and infrequent occurrence. A globally significant radiative forcing by BrC would require persistent large-scale biomass fires along with high AAE values and sufficiently high surface albedo. More probable, BrC significance may be relegated to local and regional effects due to limited lifetime, typically lower AAE values in real plumes, and the episodic nature of wildland fire. The BrC may be responsible for a local and regional climate modification. The indirect aerosol effects (aerosol cloud interaction) are clearly much more complicated and uncertain (Jacobson, 2014). The OC that is much more abundant than BC is likely to play an important role.

Acknowledgments
The research was primarily supported by U.S. DOE, Office of Science, Office of Biological and Environmental Research's Atmospheric System Research (ASR, PI MKD), and Atmospheric Radiation Monitoring (ARM) grants to LANL. M. S. and S. L. were supported as part of the Energy Exascale Earth System Model (E3SM) project and M. D. also through the Early Career Research Program. Computational resources for the E3SM simulations were provided by the PNNL Institutional Computing (PIC) facility. There are no financial conflicts of interests for any author. All data are available in Romonosky et al. (2019) and deposited at https://data.mendeley.com/datasets/fxxkmbk6yz/draft?a=0f2a1652-c9b7-46e9-9f6f-852e93263604

References

Ahmed, M., Das, M., Afser, T., Rokonujjaman, M., Akther, T., & Salam, A. (2018). Emission of carbonaceous species from biomass burning in the traditional rural cooking stove in Bangladesh. *Open J. of Air Poll.*, *7*, 287–297. https://doi.org/10.4236/ojap.2018.74014

Alexander, D., Crozierand, P. A., & Anderson, J. R. (2008). Brown carbon spheres in East Asian outflow and their optical properties. *Science*, *321*(5890), 833–836.

Bahadur, R., Praveen, P., Xu, Y., & Ramanathan, V. (2012). Solar absorption by elemental and brown carbon determined from spectral observations. *PNAS*, *109*, 17,366–17,371. https://doi.org/10.1073/pnas.1205910109

Barnard, J., Volkamer, R., & Kassianov, E. (2008). Estimation of the mass absorption cross section of the organic carbon component of aerosols in Mexico City Methropolitan Area. *Atmospheric Chemistry and Physics*, *8*(22), 6665–6679. https://doi.org/10.5194/acp-8-6665-2008

Bond, T., & Bergstrom, R. (2007). Light absorption by carbonaceous particles: Investigative review. *Aerosol Science and Technology*, *40*, 27–67. https://doi.org/10.1080/02786820500421521

Bruggeman, V. D. A. G. (1936). Berechnung verschiedener physikalischer Konstanten von heterogenen Substanzen. I. Dielektrizitätskonstanten und Leitfähigkeiten der Mischkörper aus isotropen Substanzen. *Annalen der Physik*, *416*, 636–664.

Cappa, C., Zhang, X., Russell, L. M., Collier, S., Lee, A. K., Chen, C. L., et al. (2019). Light absorption by ambient black and brown carbon and its dependence on black carbon coating state for two California, USA, cities in winter and summer. *Journal of Geophysical Research: Atmospheres*, *124*, 1550–1577. https://doi.org/10.1029/2018JD029501

Cappa, C. D., Onasch, T. B., Massoli, P., Worsnop, D. R., Bates, T. S., Cross, E. S., et al. (2012). Radiative absorption enhancements due to the mixing state of atmospheric black carbon. *Science*, *337*(6098), 1078–1081. https://doi.org/10.1126/science.1223447

Chakrabarty, R., Gyawali, M., Yatavelli, R. L., Pandey, A., Watts, A. C., Knue, J., et al. (2016). Brown carbon aerosols from burning of boreal peatlands: Microphysical properties, emission factors, and implications for direct radiative forcing. *Atmospheric Chemistry and Physics*, *16*(5), 3033–3040. https://doi.org/10.5194/acp-16-3033-2016

Chakrabarty, R., Moosmüller, H., Chen, L. W., Lewis, K., Arnott, W. P., Mazzoleni, C., et al. (2010). Brown carbon in tar balls from smoldering biomass combustion. *Atmospheric Chemistry and Physics*, *10*(13), 6363–6370. https://doi.org/10.5194/acp-10-6363-2010

China, S., Scarnato, B., Owen, R. C., Zhang, B., Ampadu, M. T., Kumar, S., et al. (2015). Morphology and mixing state of aged soot particles at a remote marine free troposphere site: Implications for optical properties. *Geophysical Research Letters*, *42*, 1243–1250. https://doi.org/10.1002/2014GL062404

Chylek, P., & Coakley, J. (1974). Aerosol and Climate. *Science*, *183*, 75–77.

Chylek, P., & Srivastava, V. (1983). Dielectric constant of a composite inhomogeneous medium. *Physical Review B*, *27*(8), 5098–5106. https://doi.org/10.1103/PhysRevB.27.5098

Chylek, P., Srivastava, V., Pinnick, R., & Wang, R. (1988). Scattering of electromagnetic waves by composite spherical particles: Experiment and effective medium approximations. *Applied Optics*, *27*(12), 2396–2404. https://doi.org/10.1364/AO.27.002396

Chylek, P., Videen, G., Geldart, W., Dobbie, S., & Tso, W. (2000). Effective medium approximations for heterogeneous particles. In M. Mishchenko, J. Hovenier, & L. Travis (Eds.), *Light Scattering by Nonspherical Particles*. London: Academic Press. Chapter 9, 273–308

Chylek, P., Videen, G., Ngo, D., Pinnick, R., & Klett, J. (1995). Effect of black carbon on the optical properties and climate forcing of sulfate aerosols. *Journal of Geophysical Research*, *100*(D8), 16325–16332. https://doi.org/10.1029/95JD01465

Chylek, P., & Wong, J. (1995). Effect of absorbing aerosols on global radiation budget. *Geophysical Research Letters*, *22*(8), 929–931. https://doi.org/10.1029/95GL00800

Coakley, J., & Chylek, P. (1975). 2-stream approximation in radiative transfer including angle of incident radiation. *Journal of the Atmospheric Sciences*, *32*, 409–418.

Cross, E. S., Onasch, T. B., Ahern, A., Wrobel, W., Slowik, J. G., Olfert, J., et al. (2010). Soot particle studies—Instrument inter-comparison—Project overview. *Aerosol Science and Technology*, *44*(8), 592–611. https://doi.org/10.1080/02786826.2010.482113

Curci, G., Alyuz, U., Barò, R., Bianconi, R., Bieser, J., Christensen, J. H., et al. (2019). Modelling black carbon absorption of solar radiation: Combining external and internal mixing assumptions. *Atmospheric Chemistry and Physics*, *19*(1), 181–204. https://doi.org/10.5194/acp-19-181-2019

Draine, B. T., & Flatau, P. (1994). Discrete-dipole approximation for scattering calculations. *Journal of the Optical Society of America. A*, *11*(4), 1491–1499. https://doi.org/10.1364/JOSAA.11.001491

Dubovik, O., Holben, B., Eck, T. F., Smirnov, A., Kaufman, Y. J., King, M. D., et al. (2002). Variability of absorption and optical properties of key aerosol types observed in worldwide location. *Journal of the Atmospheric Sciences*, *59*(3), 590–608. https://doi.org/10.1175/1520-0469(2002)059<0590:VOAAOP>2.0.CO;2

Feng, Y., Ramanathan, V., & Kotamarthi, V. (2013). Brown carbon: A significant atmospheric absorber of solar radiation? *Atmospheric Chemistry and Physics*, *13*(17), 8607–8621. https://doi.org/10.5194/acp-13-8607-2013

Fierce, L., Riemer, N., & Bond, T. (2017). Toward reduced representation of mixing state for simulating aerosol effects on climate. *Bulletin of the American Meteorological Society*, *98*(5), 971–980. https://doi.org/10.1175/BAMS-D-16-0028.I

Forrister, H., Liu, J., Scheuer, E., Dibb, J., Ziemba, L., Thornhill, K. L., et al. (2015). Evolution of brown carbon in wildfire plumes. *Geophysical Research Letters*, *42*, 4623–4630. https://doi.org/10.1002/2015GL063897

Golaz, J.-C., Caldwell, P. M., van Roekel, L. P., Petersen, M. R., Tang, Q., Wolfe, J. D., et al. (2019). The DOE E3SM coupled model version 1: Overview and evaluation at standard resolution. *Journal of Advances in Modeling Earth Systems*, *11*(7), 2089–2129. https://doi.org/10.1029/2018MS001603

Gomez, S., Carrico, C. M., Allen, C., Lam, J., Dabli, S., Sullivan, A. P., et al. (2018). Southwestern US biomass burning smoke hygroscopicity: The role of plant phenology, chemical composition, and combustion properties. *Journal of Geophysical Research: Atmospheres*, *123*(10), 5416–5432. https://doi.org/10.1029/2017JD028162

Habib, Z., & Vervisch, P. (1988). On the refractive index of soot at flame temperature. *Combustion Science and Technology*, *59*(4-6), 261–274. https://doi.org/10.1080/00102208808947100

He, C., Takano, Y., Liou, K.-N., Yang, P., Li, Q., & Mackowski, D. (2016). Intercomparison of the GOS approach, superposition T-matrix method, and laboratory measurements for black carbon optiocal properties during aging. *Journal of Quantitative Spectroscopy and Radiation Transfer*, *184*, 287–296. https://doi.org/10.1016/j.jqsrt.2016.08.004

Hobbs, P., Reid, J., Kotchenruther, R., Ferek, R., & Weiss, R. (1997). Direct radiative forcing by smoke from biomass burning. *Science*, *275*(5307), 1776–1778. https://doi.org/10.1126/science.275.5307.1777

Jacobson, M. (2014). Effects of biomass burning on climate, accounting for heat and moisture fluxes, black and brown carbon, and cloud absorption effects. *Journal of Geophysical Research: Atmospheres*, *119*, 8980–9002. https://doi.org/10.1002/2014JD021861

Kahnert, M., Nousiainen, T., Lindqvist, H., & Ebert, M. (2012). Optical properties of light absorbing carbon aggregates mixed with sulfate: Assessment of different model geometries for climate forcing calculations. *Optics Express*, *20*(9), 10045.

Kanngiesser, G., & Kahnert, M. (2018). Calculation of optical properties of light absorbing carbon with weakly absorbing coating: A model with tunable transition from film-coating to spherical-shell coating. *Journal of Quantitative Spectroscopy and Radiation Transfer*, *216*, 17–36. https://doi.org/10.1016/jqsrt.2018.05.014

Kirchstetter, T., Novakov, T., & Hobbs, P. (2004). Evidence that the spectral dependence of light absorption by aerosols is affected by organic carbon. *Journal of Geophysical Research*, *109*, D21208. https://doi.org/10.1029/2004JD004999

Lack, D., & Cappa, C. (2010). Impact of brown and clear carbon on light absorption enhancement, single scatter albedo and absorption wavelength dependence of black carbon. *Atmospheric Chemistry and Physics*, *10*, 4207–4220. https://doi.org/10.5194/acp-10-4207-2010

Lack, D., Cappa, C. D., Covert, D. S., Baynard, T., Massoli, P., Sierau, B., et al. (2008). Bias in filter based aerosol light absorption measurements due to organic aerosol loading: Evidence from ambient measurements. *Aerosol Science and Technology*, *42*(12), 1033–1041. https://doi.org/10.1080/02786820802389277

Lack, D., & Landridge, J. (2013). On the attribution of black and brown carbon light absorption using the Ångström exponent. *Atmospheric Chemistry and Physics*, *13*, 10,535–10,543. https://doi.org/10.5194/acp-13-10535-2013

Lack, D., Langridge, J., Bahreini, R., Cappa, C., Middlebrook, A., & Schwarz, J. (2012). Brown carbon and internal mixing in biomass burning particles. *PNAS*, *109*, 14,802–14,807. https://doi.org/10.1073/pnas.1206575109

Lesins, G., Chýlek, P., & Lohmann, U. (2002). A study of internal and external mixing scenarios and its effect on aerosol optical properties and direct radiative forcing. *Journal of Geophysical Research, Atmospheres*, *107*, 4094. https://doi.org/10.1029/2001JD000973

Lewis, K., Arnott, W., Moosmuller, H., & Wold, C. (2008). Strong spectral variation of biomass smoke light absorption and single scattering albedo observed with a novel dual-wavelength photoacoustic instrument. *Journal of Geophysical Research*, *113*, D16203. https://doi.org/10.1029/2007jd009699

Liu, C., Chung, C., Yin, Y., & Schnaiter, M. (2018). The absorption Ångström exponent of black carbon: From numerical aspects. *Atmospheric Chemistry and Physics*, *18*, 6259–6273. https://doi.org/10.5194/acp-18-6259-2018

Liu, C., Panetta, R., & Yang, P. (2014). Inhomogeneity structure and the applicability of effective medium approximations in calculating light scattering by inhomogeneous particles. *Journal of Quantitative Spectroscopy and Radiation Transfer*, *146*, 331–348. https://doi.org/10.1016/j.jqsrt.2014.03.018

Liu, J., Scheuer, E., Dibb, J., Ziemba, L. D., Thornhill, K. L., Anderson, B. E., et al. (2014). Brown carbon in the continental troposphere. *Geophysical Research Letters*, *41*, 2191–2195. https://doi.org/10.1002/2013GL058976

Liu, S., Aikaen, C., Arata, M., Dubey, C., Stockwell, R., Yokelson, E., et al. (2014). Aerosol single scattering albedo dependence on biomass combustion efficiency: Laboratory and field studies. *Geophysical Research Letters*, *41*, 742–748. https://doi.org/10.1002/2013GL058392

Liu, S., Aiken, A. C., Gorkowski, K., Dubey, M. K., Cappa, C. D., Williams, L. R., et al. (2015). Enhanced light absorption by mixed source black and brown carbon particles in UK winter. *Nature Communications*, *6*(1), 8435. https://doi.org/10.1038/ncomms9435

Lu, Z., Streets, D. G., Winijkul, E., Yan, F., Chen, Y., Bond, T. C., et al. (2015). Light absorption properties and radiative effects of primary organic aerosol emissions. *Environmental Science and Technology*, *49*(8), 4868–4877. https://doi.org/10.1021/acsestSb00211

Ma, X., von Salzen, K., & Li, J. (2008). Modelling sea salt aerosol and its direct and indirect effects on climate. *Atmospheric Chemistry and Physics*, *8*(5), 1311–1327. https://doi.org/10.5194/acp-8-1311-2008

Martin, S., Artaxo, P., Machado, L., Manzi, A. O., Souza, R. A. F., Schumacher, C., et al. (2017). The Green Ocean Amazon experiment (GOAmazon2014/5) observes pollution affecting gases, aerosols, clouds, and rainfall over the rain forest. *Bulletin of the American Meteorological Society*, *98*(5), 981–997. https://doi.org/10.1175/bams-d-15-00221.1

Martins, J., Hobbs, P., Weiss, R., & Artaxo, P. (1998). Sphericity and morphology of smoke particles from biomass burning in Brazil. *Journal of Geophysical Research*, *103*(D24), 32,051–32,057. https://doi.org/10.1029/98JD01153

Maxwell, G. J. C. (1904). Colours in metal glasses and metal films. *Philos. Trans. R. Soc. 833 London, Sect. A*, *3*, 385–420.

McClure, C., Lim, C., Hagan, D., Kroll, J., & Cappa, C. (2019). Biomass burning derived from a wide variety of fuels: Part 1: Properties of primary particles. *Atmospheric Chemistry and Physics Discussions*, *n/a*, 1–37. https://doi.org/10.5194/acp-2019-707

Mishchenko, M. (2014). *Electromagnetic Scattering by Particles and Particle Groups*. Cambridge: Cambridge University Press.

Mishchenko, M., Lacis, A., Carlson, B., & Travis, L. (1995). Nonsphericity of dust-like tropospheric aerosols: Implications for aerosol remote sensing and climate modeling. *Geophysical Research Letters*, *22*(9), 1077–1080. https://doi.org/10.1029/95GL00798

Moosmuler, H., & Sorensen, C. M. (2018a). Small and large particle limits of single scattering albedo for homogeneous, spherical particles. *Journal of Quantitative Spectroscopy & Radiative Transfer*, *204*, 250–255. https://doi.org/10.1016/j.jqsrt.2017.09.029

Moosmuler, H., & Sorensen, C. M. (2018b). Single scattering albedo of homogeneous, spherical particles in the transition region. *Journal of Quantitative Spectroscopy & Radiative Transfer*, *219*, 333–338. https://doi.org/10.1016/j.jqsrt.2018.08.015

Moosmuller, H., Chakrabarty, R., & Arnott, W. (2009). Aerosol light absorption and its measurement: A review. *Journal of Quantitative Spectroscopy and Radiation Transfer*, *110*(11), 844–878. https://doi.org/10.1016/j.jqsrt.2009.02.035

Pokhrel, R., Wagner, N. L., Langridge, J. M., Lack, D. A., Jayarathne, T., Stone, E. A., et al. (2016). Parameterization of single-scattering albedo (SSA) and absorption Ångström exponent (AAE) with EC/OC for aerosol emissions from biomass burning. *Atmospheric Chemistry and Physics*, *16*(15), 9549–9561. https://doi.org/10.5194/acp-16-9549-2016

Rasch, P. J., Xie, S., Ma, P. L., Lin, W., Wang, H., Tang, Q., et al. (2019). An overview of the atmospheric component of the Energy Exascale Earth System Model. *Journal of Advances in Modeling Earth Systems*, *11*(8), 2377–2411. https://doi.org/10.1029/2019MS001629

Rissler, J., Vestin, A., Swietlicki, E., Fisch, G., Zhoui, J., Artaxo, P., & Andrea, M. (2006). Size distribution and hygroscopic properties of aerosol particles from dry-season biomass burning in Amazonia. *Atmospheric Chemistry and Physics*, *6*(2), 471–491. https://doi.org/10.5194/acp-6-471-2006

Romonosky, D., Gomez, S., Lam, J., Carrico, C., Aiken, A., Chylek, P., & Dubey, M. (2019). Optical properties of laboratory and ambient biomass burning aerosols: Elucidating black, brown, and organic carbon components and mixing regimes. *Journal of Geophysical Research: Atmospheres*, *124*, 5088–5105. https://doi.org/10.1029/2018JD029892

Russell, P., Bergstrom, R. W., Shinozuka, Y., Clarke, A. D., DeCarlo, P. F., Jimenez, J. L., et al. (2010). Absorption Ångström exponent in AERONET and related data as an indicator of aerosol composition. *Atmospheric Chemistry and Physics*, *10*(3), 1155–1169. https://doi.org/10.5194/acp-10-1155-2010

Saleh, R., Cheng, Z., & Atwi, K. (2018). The brown-black continuum of light-absorbing combustion aerosols. *Environmental Science & Technology Letters*, *5*, 508–513. https://doi.org/10.1021/acs.estlett.8b00305

Saleh, R., Hennigan, C. J., McMeeking, G. R., Chuang, W. K., Robinson, E. S., Coe, H., et al. (2013). Absorptivity of brown carbon in fresh and photo-chemically aged biomass-burning emissions. *Atmospheric Chemistry and Physics*, *13*(15), 7683–7693. https://doi.org/10.5194/acp-13-7683-2013

Saleh, R., Robinson, E. S., Tkacik, D. S., Ahern, A. T., Liu, S., Aiken, A. C., et al. (2014). Brownness of organics in aerosols from biomass burning linked to their black carbon content. *Nature Geoscience*, *7*(9), 647–650. https://doi.org/10.1038/ngeo2220

Schmid, O., Artaxo, P., Arnott, W. P., Chand, D., Gatti, L. V., Frank, G. P., et al. (2006). Spectral light absorption by ambient aerosols influenced by biomass burning in the Amazon Basin. I: Comparison and field calibration of absorption measurement techniques. *Atmospheric Chemistry and Physics*, *6*(11), 3443–3462. https://doi.org/10.5194/acp-6-3443-2006

Schmid, O., Chand, D., Karg, E., Guyon, P., Frank, G.. P., Swietlicki, E., & Andreae, M. O. (2009). Derivation of density and refractive index of organic matter and elemental carbon from closure between physical and chemical aerosol properties. *Environmental Science & Technology*, *43*(4), 1166–1172. https://doi.org/10.1021/es800570p

Schuster, G., Dubovik, O., Arola, A., Eck, T., & Holben, B. (2016). Remote sensing of soot carbon - Part 2: Understanding the absorption Angstrom exponent. *Atmospheric Chemistry and Physics*, *16*, 15879–1602. https://doi:10.5194/acp-16-1587-2016

Sengupta, D., Samburova, V., Bhattarai, C., Kirillova, E., Mazzoleni, L., Iaukea-Lum, M., et al. (2018). Light absorption by polar and non-polar aerosol compounds from laboratory biomass combustion. *Atmospheric Chemistry and Physics*, *18*(15), 10,849–10,867. https://doi.org/10.5194/acp-18-10849-2018

Shrivastava, M., Easter, R. C., Liu, X., Zelenyuk, A., Singh, B., Zhang, K., et al. (2015). Global transformation and fate of SOA: Implications of low-volatility SOA and gas-phase fragmentation reactions. *Journal of Geophysical Research: Atmospheres*, *120*, 4169–4195. https://doi.org/10.1002/2014JD022563

Sorensen, C. M., Maughan, J. B., & Moosmuller, H. (2019). Spherical particle absorption over a broad range of imaginary refractive index. *Journal of Quantitative Spectroscopy and Radiative Transfer*, *226*, 81–86. https://doi.org/10.1016/j.jqsrt.2019.01.011

Sumlin, B. J., Heinson, Y. W., Shetty, N., Pandey, A., Pattison, R. S., Baker, S., et al. (2018). UV-Vis-IR spectral complex refractive indices and optical properties of brown carbon aerosol from biomass burning. *Journal of Quantitative Spectroscopy & Radiative Transfer*, *206*, 392–398. https://doi.org/10.1016/j.jqsrt.2017.12.009

Torok, S., Malmborg, V. B., Simonsson, J., Eriksson, A., Martinsson, J., Mannazhi, M., et al. (2018). Investigation of the absorption Ångström exponent and its relation to physicochemical properties for mini-CAST soot. *Aerosol Science and Technology*, *52*(7), 757–767. https://doi.org/10.1080/02786826.2018.1457767

Videen, G., & Chylek, P. (1998). Scattering by a composite sphere with an absorbing inclusion and effective medium approximations. *Optics Communication*, *158*, 1–6. https://doi.org/10.1016/S0030-4018(98)00557-4

Videen, G., Ngo, D., Chylek, P., & Pinnick, R. (1995). Light scattering from a sphere with an irregular inclusion. *Journal of the Optical Society of America*, *12*(5), 922–928. https://doi.org/10.1364/JOSAA.12.000922

Wang, X., Heald, C. L., Ridley, D. A., Schwarz, J. P., Spackman, J. R., Perring, A. E., et al. (2014). Exploiting simultaneous observational constrains on mass and absorption to estimate the global direct radiative forcing of black and brown carbon. *Atmospheric Chemistry and Physics Discussions*, *14*(11), 17,527–17,583. https://doi.org/10.5194/acpd-14-17527-2014

Winter, B., & Chylek, P. (1997). Contribution of sea salt aerosol to the planetary clear-sky albedo. *Tellus*, *49B*, 72–79.

Yang, P., Ding, J., Panetta, R. L., Liou, K.-N., Kattawar, G. W., & Mishchenko, M. I. (2019). On the convergence of numerical computations for both exact and approximate solutions for electromagnetic scattering by nonspherical dielectric particles. *Progress In Electromagnetics Research*, *164*, 27–61. https://doi.org/10.2528/PIER18112810

Zhang, G., Peng, L., Lian, X., Lin, Q., Bi, X., Chen, D., et al. (2018). An improved absorption Ångström exponent (AAE)-based method for evaluating the contribution of light absorption from brown carbon with a high time resolution. *Aerosol and Air Quality Research*, *19*(1), 15–24. https://doi.org/10.4209/aaqr.2017.12.0566

Zuidema, P., Sedlacek, A. J. III, Flynn, C., Springston, S., Delgadillo, R., Zhang, J., et al. (2018). The Ascension Island boundary layer in the remote southeast Atlantic is often smoky. *Geophysical Research Letters*, *45*, 4456–4465. https://doi.org/10.1002/2017GL076926